LANGMUIR

pubs.acs.org/Langmuir Article

A Platform Approach for Designing Sustainable Indole Thiosemicarbazone Corrosion Inhibitors with Enhanced Adsorption Properties

A. K. S. Koushik,◆ Demetrius Finley,◆ Nadia N. Intan, Lucas J. Showman, Kyle Podolak, Zachery Crandall, Theresa L. Windus, Jim Pfaendtner, Siegfried R. Waldvogel, George A. Kraus,* and Jean-Philippe Tessonnier*

Cite This: *Langmuir* 2025, 41, 8407−8423 Read Online

ACCESS | Metrics & More | Article Recommendations | Supporting Information

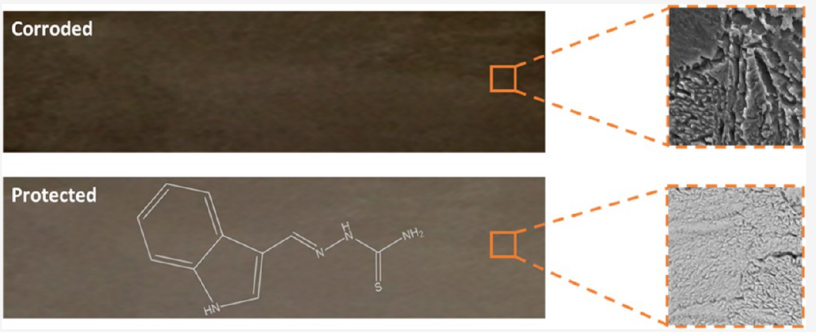

ABSTRACT: With an estimated global cost of $2.5 trillion per year, metal corrosion represents a major challenge across all industrial sectors. Numerous inorganic and organic corrosion inhibitors have been developed, but there are growing concerns about their toxicity and impact on the environment. Here, superior organic corrosion inhibitors based on indole-3-carboxaldehyde, a compound commonly found in the digestive system, and thiosemicarbazones, a safe class of ligands, were designed and studied for mild steel in pH 1 sulfuric acid solutions. Electroanalytical techniques and gravimetric tests revealed inhibition efficiencies as high as 98.9% at 30 °C. Models using Langmuir isotherms gave adsorption equilibrium constants K_{ads} of 2 to 9 × 10^4 M^{-1} and corresponding Gibbs free energies of adsorption (ΔG_{ads}) as high as −41.44 kJ mol^{-1}, indicating their chemisorption. SEM images confirmed the efficacy of these corrosion inhibitors, as surface features showed limited to no changes after tests. Surface analysis by XPS and LC-MS revealed inhibitor concentrations on the order of 0.7 to 1.8 μg cm^{-2} for the best compounds, further underlining their performance at low concentrations. Mapping of the surface by MALDI-MS further confirmed the homogeneous coating of the steel surface, with no visible fluctuations in concentrations. As all inhibitors shared the same indole thiosemicarbazone platform, unique structure−performance relationships were drawn from theoretical calculations. Notably, DFT and AIMD explained the differences in performance, highlighting the role of side groups in the distribution of the molecular orbitals and the role of water molecules in enhancing the electronic properties of the organic corrosion inhibitors and promoting their chemisorption.

1. INTRODUCTION

Mild steel stands as one of the most prevalent construction materials, finding applications in various sectors, including construction, energy, manufacturing, and transportation. Its utilization is particularly pronounced in the energy sector, where it serves in the fabrication of pipelines, containers, and related infrastructure, primarily due to its cost-effectiveness and robust mechanical properties.[1−3] However, its corrosion remains a major challenge, especially in the case of pipelines. The transportation and storage of crude oil, which is filled with copious minerals, often results in the accumulation of deposits along the pipelines and containers, causing their blockage.[4,5] To suppress such deposits, the oil industry utilizes an array of processes that include acid pickling and descaling, where potent acids, such as hydrochloric acid (HCl) and sulfuric acid (H_2SO_4), are employed to dissolve the inorganic deposits. Although these processes are effective in cleaning the pipelines, they also affect mild steel, which is prone to corrosion in the presence of strong acids.[6,7]

Received: January 10, 2025
Revised: February 28, 2025
Accepted: March 11, 2025
Published: March 24, 2025

Corrosion inhibitors play a vital role in protecting and preventing the deterioration of mild steel. Traditionally, pipelines are protected by the application of inorganic coatings that contain compounds such as chromates, molybdates, etc.[8−10] However, these compounds are carcinogenic and detrimental to the environment. To mitigate these concerns, research has gravitated toward the design of safe and environmentally friendly organic corrosion inhibitors.[11−13] Recent studies have shown that aromatic compounds incorporating heteroatoms (N, O, S, etc.) typically give promising results.[14,15] The derivatives of aromatic molecules, such as pyrroles,[16−18] pyridines,[5,19,20] imidazole,[21−24] triazole,[25−28] thiazole,[14,29,30] quinazolinone,[31−33] etc., have been reported to have good to excellent inhibition efficiency against mild steel corrosion. Their efficacy is primarily ascribed to their ability to interact with the mild steel surface through physisorption or chemisorption, processes facilitated by the sharing of electrons with the vacant 3d orbitals of iron (Fe) atoms at the surface.[34,35] However, their innocuousness has recently been challenged, and some of these organic compounds have been revealed to be harmful to the environment. Hence, new strategies for the synthesis of eco-friendly inhibitors need to be outlined and explored.[36,37] Biobased inhibitors derived from natural resources using microorganisms are particularly promising as they are typically biodegradable and nontoxic, offering a sustainable alternative to inorganic and fossil-derived inhibitors.

Here, we designed a new generation of corrosion inhibitors derived from indole-3-carboxaldehyde, a compound commonly found in human and animal digestive systems resulting from the bacterial degradation of L-tryptophan, one of the most prevalent dietary amino acids.[38,39] Rather than following the Edisonian method of trial and error, we used the indole structure as a platform that we derivatized to generate a set of structurally similar molecules. Our goal in this study, in addition to generating a new class of performance corrosion inhibitors, is to demonstrate the potential of this research strategy to establish structure−activity relationships, offer a more systematic and predictive framework for designing effective and targeted inhibitors, and generate data sets that could inform future computational tools and machine learning (ML)-guided research.

To enhance the performance of the biosourced indole, its aldehyde function was leveraged to couple thiosemicarbazones, a low-cost and widely available class of organosulfur compounds that find applications as metal ligands in coordination chemistry and as a safe family of antitumoral and antiparasitic drugs in medicine.[40] The structural diversity of thiosemicarbazones, specifically the possibility to tune their side groups, enabled us to synthesize a wide range of indole derivatives using an elegant and environmentally benign 2-step synthesis. The obtained compounds were subsequently evaluated as corrosion inhibitors for mild steel by using various electroanalytical, gravimetric, and spectroscopic techniques. Corrosion inhibitions as high as 98.9% were achieved, surpassing the performance of the best organic inhibitors reported to date. Gravimetric tests and Langmuir isotherms further substantiated the electroanalytical findings, revealing Gibbs free energies exceeding −40 kJ/mol. The results underscored that chemisorption is the dominant mechanism governing the interaction between the mild steel surface and the designed inhibitor molecules.[41] Density functional theory (DFT) and ab initio molecular dynamics (AIMD) calculations highlighted the dominant parameters that control the inhibitors' performance as well as the role of solvation on the electronic structure of the organic molecules.

2. EXPERIMENTAL SECTION

2.1. Synthesis of the Organic Corrosion Inhibitors. All starting chemicals were purchased from Sigma-Aldrich, Oakwood Chemical, and Alfa Aesar; solvents were purchased from Fisher Scientific and used without further purification. All reactions were carried out in flame-dried glassware under argon with dry solvents under anhydrous conditions unless otherwise stated. A solution of either indole-3-carboxaldehyde (0.4935 g; 3.4 mmol) or 5-methoxyindole-3-carboxaldehyde (0.5956 g; 3.4 mmol) was prepared in 22 mL of ethanol. Thiosemicabazide (0.483 g, 5.3 mmol) was subsequently added, and the solution was refluxed at 85 °C for 4 h. Once the mixture was cooled, the ethanol was removed by vacuum. The residue was then washed with 25 mL of 1 N HCl and 25 mL of deionized water and dried in high vacuum. The indole-substituted inhibitors were synthesized using a slightly different method, starting with a solution of indole (2.343 g; 20 mmol) in dry dimethylformamide (DMF) to which 0.88 g of NaH (22 mmol) was added at 0 °C. After the mixture was stirred for 30 min at 0 °C, 2.748 g (24 mmol) of 2-chloropyrimidine was added to the mixture. The solution was then heated with vigorous stirring to 130 °C and kept at this temperature for 24 h. The solution was then cooled to room temperature, poured into water, and extracted with ethyl acetate. The organic phase was then concentrated and purified by flash column chromatography. In a second step, the substituted indole was reacted with $POCl_3$ in DMF under argon at 0 °C. The reaction mixture was slowly brought to room temperature and stirring was continued for another 2 h. Once the reaction mixture was completed, it was poured into cold saturated sodium bicarbonate and stirred for 30 min. A solid precipitated out and was collected by filtration. The solid was then washed with H_2O and hot hexane to afford the desired product with 90% yield.

All of the organic corrosion inhibitors were purified either by recrystallization or flash column chromatography using silica gel 60 Å with a particle size of 0.032−0.063 mm. ^{1}H nuclear magnetic resonance (NMR) spectra of the recovered products were acquired in $CDCl_3$ or DMSO-d6 by using a Varian MR-400 (400 MHz) or Bruker NEO 400 (400 MHz) spectrometer. The corresponding spectra and ^{1}H chemical shifts (δ) given in ppm relative to the residual protonated chloroform peak or dimethyl sulfoxide peak as an internal reference are provided in the Supporting Information. High-resolution mass spectra (HRMS) were recorded on an Agilent 6540 QTOF (quadrupole time-of-flight) mass spectrometer by using electrospray ionization. All yields refer to isolated products by either silica gel chromatography or recrystallization.

2.2. Preparation of Mild Steel Samples. Mild steel A366/1008 sheets (Fe-99.39%, Mn-0.38%, C-0.07%, Al-0.045%, Cr-0.024%, Ni-0.02%, others) were purchased from Online Metals and cut into 1 × 3 × 0.076 cm coupons. The coupons were manually polished with 600, 800, 1200, and 2000-grade sandpaper and subsequently sonicated in ethanol to remove any steel dust formed during the polishing process. After cleaning, the samples were wiped and placed in a drying oven at 60 °C for 30 min to evaporate any excess ethanol. Insulating tape was thoroughly placed on the front and back sides of the dried coupons to decrease the exposed metal surfaces to squares of 1 cm^2 each. The active corrosive surface area, including all sides, was 2.228 cm^2.

2.3. Electrochemical Analysis. Open circuit voltammetry (OCV), electrochemical impedance spectroscopy (EIS), and potentiodynamic polarization were employed to characterize the corrosion behavior of the mild steel coupons in 0.1 M H_2SO_4 (Sigma-Aldrich, research grade). It was reported in the literature that the rate of corrosion is higher in H_2SO_4 when compared to HCl for similar concentrations, so H_2SO_4 was chosen as a corroding medium.[19] A single-compartment 3-electrode system was utilized, with mild steel coupons acting as the working electrode, a platinum coil as the counter electrode, and an Ag/AgCl electrode saturated in 4 M KCl as the reference electrode (Pine Research Instrumentation). The electrolyte was freshly prepared before each experiment by dissolving 1 mM of organic inhibitor in 50 mL of 0.1

https://doi.org/10.1021/acs.langmuir.5c00183
Langmuir 2025, 41, 8407−8423

M H_2SO_4 using a tip sonicator for 15 min (Branson 450 Digital Sonifier with a tip size of 0.5 in. and operated at 50% amplitude). All of the electrochemical measurements were performed using a Biologic VSP 300 potentiostat equipped with the EC-LAB software. Prior to every measurement, the electrolyte was purged with Argon for 30 min to remove any dissolved oxygen from the solution, and an Ar atmosphere was maintained throughout the analysis to ensure inert conditions. The electrochemical cell was placed in a water bath at 30 °C and maintained at this temperature throughout the experiment. OCV measurements were initially conducted for 30 min to stabilize the system, followed by EIS measurements in the frequency range of 0.1 MHz to 0.1 Hz using an amplitude of 10 mV at open circuit potential. Finally, potentiodynamic polarization measurements were performed in the range of ±500 mV of open circuit potential, with a scan rate of 50 mV s^{-1}. All electrochemical experiments were performed in triplicate to ensure reproducibility. The error was calculated as the deviation from the mean, expressed as a percentage of the mean. The error was found to be less than 0.4% for all of the measurements.

2.4. Gravimetric Analysis. Gravimetric tests were performed to study the weight change of mild steel coupons during the corrosion process in the presence and absence of organic corrosion inhibitors. Mild steel coupons were completely immersed in 0.1 M H_2SO_4 for 3 h at various temperatures (30, 35, 40, 45, and 50 °C) and different concentrations of corrosion inhibitor (1, 0.8, 0.6, 0.4. 0.2, and 0 mM). These conditions were selected to ensure consistency with prior studies and facilitate a careful comparison of the corrosion inhibition efficiencies with the values reported in the literature. A water bath was used to maintain a constant temperature throughout the experiment. The weights of these coupons were measured before and after corrosion, after drying using a stream of dry air, and gentle patting of the surface using a dust-free Kimwipe cloth (Kimtech, Kimberly-Clark) to remove any residual solution from the surface. All of the gravimetric experiments were performed in triplicate to ensure reproducibility, and the calculated ΔG_{ads} were well within a 2% error.

2.5. Scanning Electron Microscopy. Scanning electron microscopy (SEM) images and energy-dispersive X-ray spectra (EDS) were acquired by using a FEI Quanta 250 field-emission microscope equipped with an Oxford Aztec energy-dispersive spectrometer. SEM images of polished mild steel coupons were recorded prior to the corrosion process, while taking note of the axial position of the area of interest. These mild steel coupons were then subjected to corrosion in the presence and absence of 1 mM inhibitor in 0.1 M H_2SO_4 for a duration of 1 h at 30 °C. The corroded coupons were dried using a stream of air and gently wiped to eliminate residual acid on the surface. Finally, SEM images of the corroded coupons were recorded at the previously noted axial position to study the changes in the surface morphology of the mild steel coupons with and without inhibitors. EDS spectra were recorded for selected areas to determine the local and average elemental compositions of the surface.

2.6. Mass Spectrometry Analysis and Imaging. Mild steel coupons corroded in the presence of inhibitors and reference coupons (an uncorroded coupon and a coupon corroded in blank H_2SO_4) were submitted to the Iowa State University W.M. Keck Metabolomics Research Laboratory (RRID:SCR 017911) for LC-MS analysis. These coupons were placed in 20 mL glass tubes with Teflon-lined caps. A liquid extraction was initiated with the addition of 6 mL of 1:1:1 LC-MS grade methanol:water:acetonitrile (Fisher Scientific) for mild steel coupons corroded in IT-1, IT-2, and IT-3. For IT-4, 18 mL of 1:1:7 methanol:20 mM HCl:acetonitrile was used for the extraction solvent. Samples were then vortexed for 10 s and sonicated for 10 min in a sonicating water bath (Model 2510, Branson Ultrasonics). The vortex and sonication steps were repeated three times before the sample extracts were allowed to settle, and the extract supernatants were recovered and transferred to glass autosampler vials. Similarly, neat coupons were treated by using the same extraction solvents. The neat standards were prepared as 5 μg mL^{-1} samples for the initial LC-MS profiling. Additionally, standard curves were prepared for each inhibitor molecule, with amounts ranging from 0.33 to 133 μg per sample. After sample preparation, the sample extracts were immediately subjected to LC-MS analysis.

For imaging, mild steel coupons (uncorroded, corroded in blank H_2SO_4, corroded in the presence of inhibitor) were coated with α-cyano-4-hydroxycinnamic acid (CHCA; Sigma-Aldrich) as the matrix, which was applied using an oscillating capillary nebulizer (OCN) sprayer.[42] In short, three mild steel coupons were coated in sets of three plates at a time for three spray deposition cycles of 300 μL of 10 mg mL^{-1} CHCA in 7:3 acetonitrile:water with 1% trifluoroacetic acid; all solvents were LC-MS grade (Fisher Scientific). The coupon positions were rotated after each deposition cycle to ensure an even matrix deposition. The OCN unit was operated with a matrix solution flow rate of 2 mL h^{-1} and a nitrogen gas pressure of 70 kPa with a flow rate of 4.5 L min^{-1}. After matrix deposition, the coupons were dried in a vacuum desiccator for 30 min. Images of the prepared samples were acquired using a Bruker SolariX Fourier transform ion cyclotron resonance mass spectrometer (FT-ICR MS) equipped with matrix-assisted laser desorption ionization (MALDI). Additional experimental details are provided in the Supporting Information.

2.7. Theoretical Calculations. The molecular properties of the four indole thiosemicarbazone inhibitors were computed in both vacuum and in water solvated models using the Gaussian 16 software.[43] The calculations were done using density functional theory (DFT) at the B3LYP[44,45] hybrid functional level and the 6−31G (2df, p).[46] Water solvation was modeled implicitly by employing the self-consistent reaction field (SCRF)[47−49] module and the Onsager model reaction field calculation[50−55] consisting of the dipole polarizable continuum model (DPCM) method that was incorporated within the Gaussian 16 code, where the solute molecule was placed in a cavity within the solvent reaction field.

Using both vacuum and solvated models, the following theoretical parameters were calculated for the aforementioned molecules: (1) highest occupied molecular orbital (HOMO), (2) lowest unoccupied molecular orbitals (LUMO), (3) the Mulliken charges of these two molecular levels, (4) the bandgap that is the energy difference between HOMO and LUMO orbitals, (5) absolute electronegativity, (6) global hardness, (7) global softness, and (8) the fraction of electrons transferred from each molecule to the metal surface. The amount of the electron transferred was calculated by assuming the electronegativity of the iron metal surface (χ_{Fe} = 7.0 eV), as reported in the literature.[34]

Furthermore, ab initio molecular dynamics (AIMD) simulations were performed for IT-1 to understand the adsorption mechanism and energetics of the inhibitor molecule on the Fe surface. IT-1 was selected based on its high performance compared to other inhibitors considered in this study. The simulations were performed on the Fe (110) surface as it is one of the most dominant iron surfaces, it has the lowest surface energy,[56] and most studies on organic corrosion inhibitors focused on their adsorption on the Fe (110) facet.[34,57,58] An optimized Fe unit cell was extended to a 4 × 4 × 2 in the *x*-, *y*-, and *z*-directions, respectively, to create a supercell. The supercell was then rotated 90° in the *xy*-direction to create a surface area of 16.06 $Å^2$ in size and then cleaved in the *z*-direction to create the Fe (110) slab. The Fe unit cell, bulk, and (110) slab were all optimized with the convergence criteria of 1×10^{-5} eV for electronic self-consistent iterations until all of the forces acting on ions were less than 0.02 eV/Å. The 3 × 3 × 3 and 3 × 3 × 1 meshes of *k*-points in the Monkhorst−Pack scheme[59] were chosen for the Brillouin zone sampling of the bulk and the slab, respectively, along with the application of 0.1 eV of Gaussian smearing. Further details are provided in the Supporting Information.

The adsorption of IT-1 onto the iron surface was probed using AIMD simulations that were done at Γ-point sampling with a time step of δt = 1 fs for at least 10 ps, until all of the forces converged. A cutoff of 400 eV was also employed, with the electronic energy convergence criterion of 1×10^{-4} eV that was enforced at each time step. The Nosé-Hoover algorithm[60,61] was employed to maintain the average temperature at 300 K. In all cases, one molecule of inhibitor was put in the box, surrounded by water molecules. The effect of water on the adsorption of the inhibitors and its corresponding adsorption-free energy barriers was studied by employing two different models: (1) a water monolayer on top of the iron surface and (2) bulk water. For the monolayer, the Fe (110) slab was fitted into a simulation cell of 16.06 × 16.06 × 30.68 $Å^3$ subject to periodic boundary conditions. The *z*-length

https://doi.org/10.1021/acs.langmuir.5c00183
Langmuir 2025, 41, 8407−8423

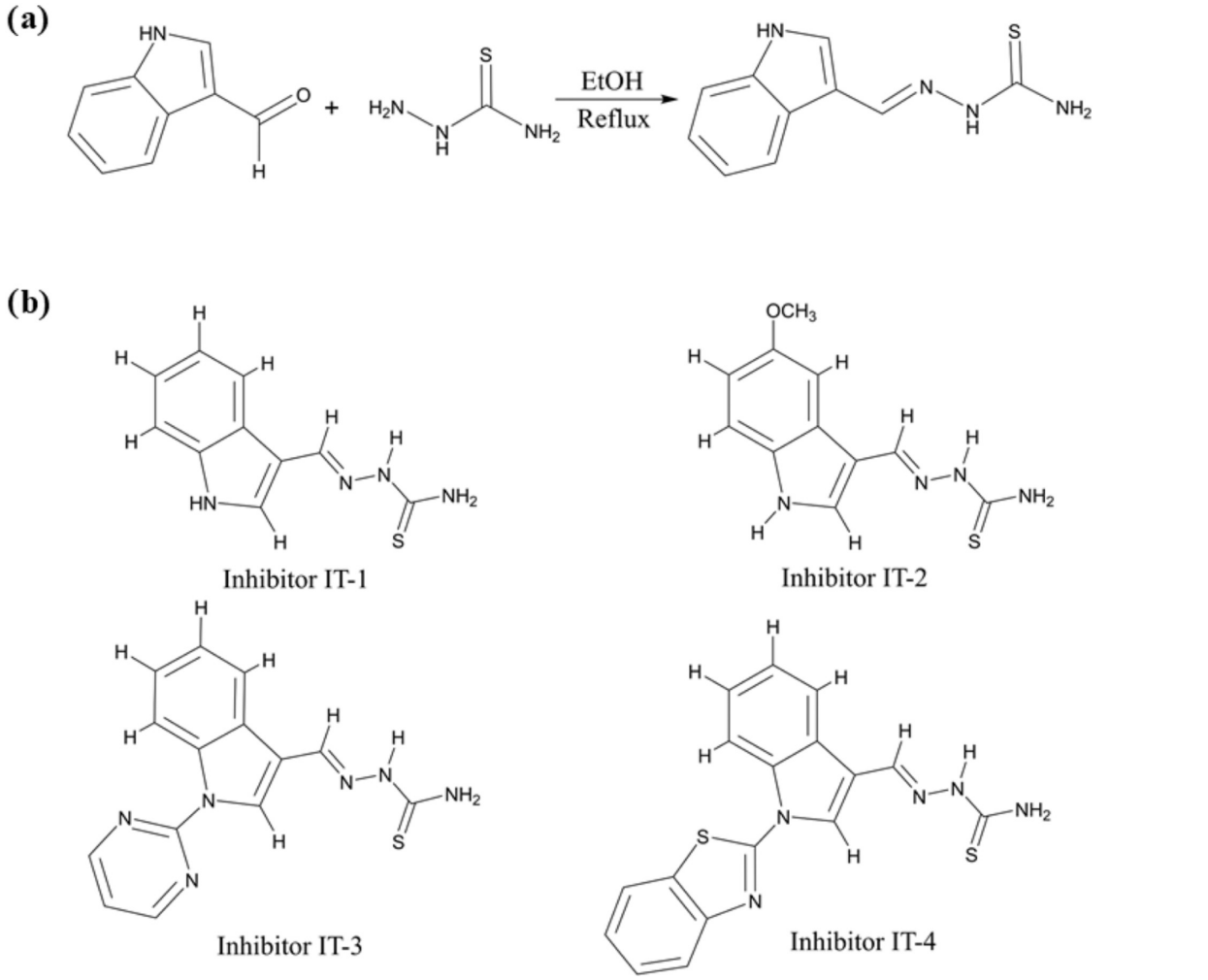

Figure 1. (a) Overall schematic of the synthesis pathway and (b) molecular structures of the indole thiosemicarbazone (IT) corrosion inhibitors.

of the simulation box leaves ~26.5 Å of a vacuum gap that was incorporated to avoid spurious interactions between adjacent slabs. The monolayer was composed of 30 water molecules that were first absorbed on the Fe (110) surface to provide a complete monolayer coverage to the slab. The density of the water monolayer in the simulation box was approximately equivalent to ρ = 0.13 g/cm^3. Meanwhile, in the case of the bulk water, the size of the simulation was reduced to 16.06 × 16.06 × 20 Å^3, which was filled with 140 water molecules to mimic the density of the water in real life that is ρ = 1 g/cm^3.

Avogadro[62] was used to visualize the HOMO and LUMO orbitals, and Visual Molecular Dynamics (VMD)[63] and Visualization for Electronic and Structural Analysis (VESTA)[64] were used for molecular dynamics trajectories analysis and image creation, respectively.

3. RESULTS AND DISCUSSION

3.1. Synthesis and Characterization. The corrosion inhibitors were synthesized using a simple and green procedure that leverages indole-3-carboxaldehyde, a product of the microbial degradation of L-tryptophan, and thiosemicarbazide, a safe and widely available organic compound key to chelating agents and to antitumoral and antiparasitic drugs (Figure 1a). Upon purification, the indole thiosemicarbazone (IT) inhibitors IT-1, IT-2, IT-3, and IT-4 were obtained in 70, 96, 75, and 69% yields, respectively (Figure 1b). The corresponding ^{1}H NMR peak assignments and HRMS data are provided in the Supporting Information.

3.2. Electrochemical Analysis. *3.2.1. Electrochemical Impedance Spectroscopy.* The electrochemical impedance of the mild steel coupons in the presence of inhibitor molecules was calculated using the Nyquist plots shown in Figure 2a. The fitting of the plots was done by approximating Randell's circuit, which consists of solution resistance (R_s) in series with a parallel arrangement of charge transfer resistance (R_{ct}) and constant phase element (CPE) as indicated in Figure 2b.[65] The corrosion parameters such as R_{ct}, double layer capacitance (C_{dl}), and inhibition efficiency (%η_R) were calculated from the equivalent circuit using eqs 1 and 2.[34,66] The corresponding values are presented in Table 1.

$$\%\eta_R = \frac{R_{ct(i)} - R_{ct(o)}}{R_{ct(i)}} \times 100 \quad (1)$$

$$C_{dl} = (Y_0 R_{ct}^{1-n})^{1/n} \quad (2)$$

From the data in Table 1, it can be observed that the charge transfer resistance (R_{ct}) increased by approximately 2 orders of magnitude in the presence of the inhibitors compared to the blank sample. This increase in the R_{ct} values indicates the formation of a protective layer on the surface of the mild steel coupon, which restricts the charge transfer between the surface and the electrolyte, thereby preventing corrosion. In addition, it can be noted that the values of C_{dl} decreased in the presence of

https://doi.org/10.1021/acs.langmuir.5c00183
Langmuir 2025, 41, 8407−8423

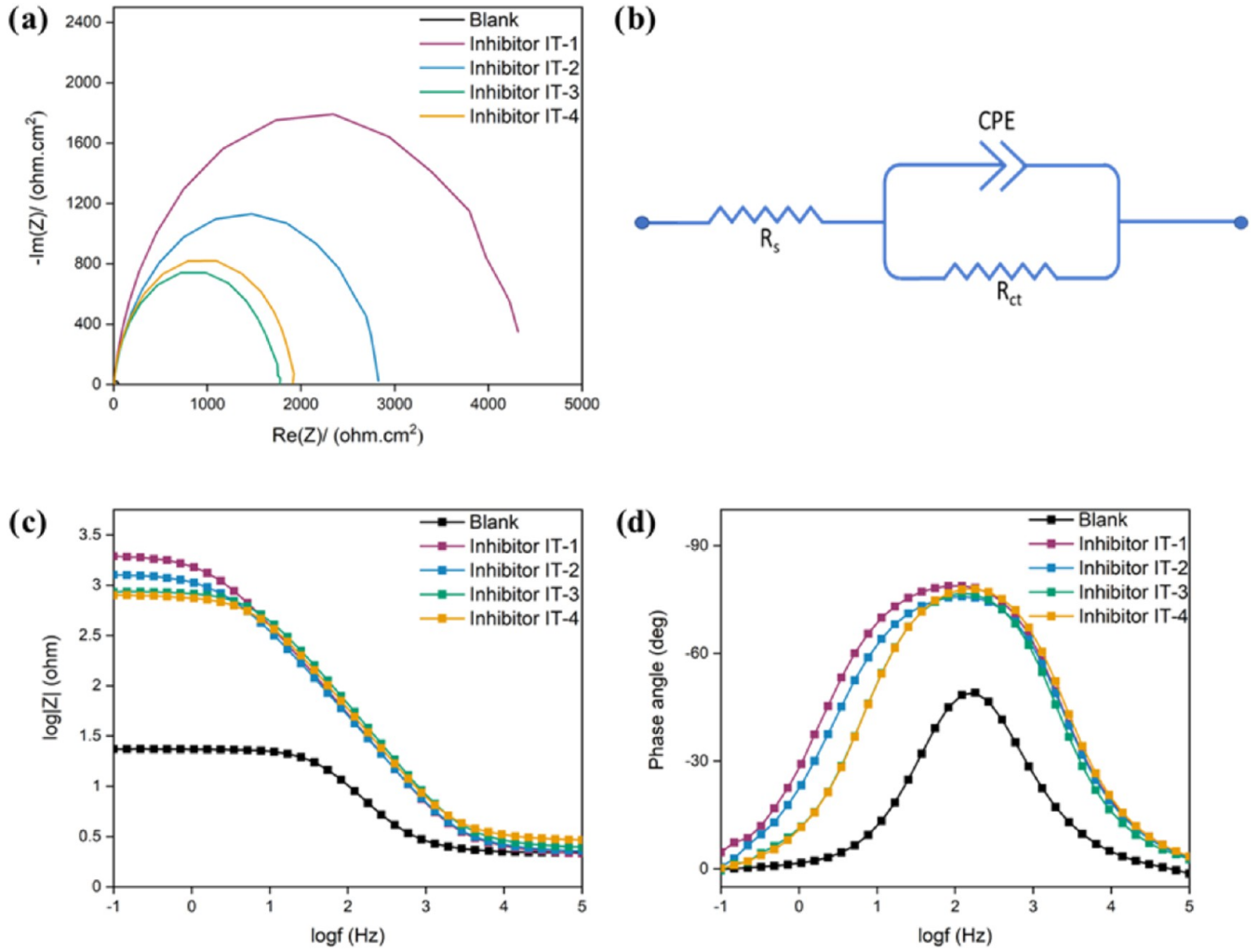

Figure 2. (a) Nyquist plot, (b) equivalent Randell's circuit, (c) Bode impedance magnitude plot, and (d) corresponding Bode phase angle plot for mild steel in 0.1 M H_2SO_4 in the absence and presence of 1 mM of IT corrosion inhibitors.

Table 1. Corrosion Parameters Calculated after Fitting the Nyquist Plot to Randell's Circuit

inhibitor	R_s (Ω cm^2)	R_{ct} (Ω cm^2)	C_{dl} (μF/cm^2)	$\%\eta_R$
blank	4.9	47.2	210.48	
IT-1	5.0	4255.5 (±0.285)	40.62	98.89 (±0.004)
IT-2	5.1	2782.8 (±0.169)	45.40	98.30 (±0.004)
IT-3	6.7	1736.3 (±0.100)	38.06	97.28 (±0.003)
IT-4	5.7	1903.2 (±0.088)	32.82	97.52 (±0.002)

inhibitors, which is due to the resulting displacement of water molecules by the organic compounds on the surface of mild steel.[34,67] The highest corrosion inhibition efficiency ($\%\eta_R$) was observed to be 98.89% for inhibitor IT-1. The $\%\eta_R$ values for inhibitors IT-2, IT-3, and IT-4 were found to be 98.30, 97.28, and 97.52%, respectively. Interestingly, the $\%\eta_R$ values for inhibitors IT-1 and IT-2 were higher than those for IT-3 and IT-4 despite the similar molecular structures of the four compounds.

The bode impedance plot presented in Figure 2c showed a clear increase in the values of interfacial impedance at all frequencies in the presence of inhibitor molecules compared with the blank sample. This further supports that the inhibitor molecules are forming a protective layer over the surface of the mild steel. The bode phase angle plot (Figure 2d) revealed that all of the curves display a single-phase maximum, signifying a single time constant for the metal-acid interface, which can be assigned to the charge transfer process. The increase in the numerical value of the phase angle in the presence of an inhibitor is due to an increase in capacitive characteristics because of the formation of a protection layer over the mild steel surface, which acts as an electric double layer.[34]

3.2.2. Potentiodynamic Polarization Curves. Polarization curves were used to calculate the corrosion parameters, such as corrosion current density (I_{corr}), corrosion potential (E_{corr}), Tafel slopes (β_a and β_c), and inhibition efficiency ($\%\eta_I$). The values of I_{corr} and E_{corr} were determined with the aid of EC-LAB software using Tafel plots and $\%\eta_I$ was calculated from these I_{corr} values by using eq 3

$$\%\eta_I = \frac{I_o - I_i}{I_o} \times 100 \tag{3}$$

It can be observed from the polarization curves presented in Figure 3 that both cathodic and anodic currents decreased in the presence of inhibitor molecules compared to the blank H_2SO_4 solution. This observation suggests that the inhibitor molecules are effective in mitigating both the hydrogen evolution reaction (HER) at the cathode and mild steel degradation at the anode,

https://doi.org/10.1021/acs.langmuir.5c00183
Langmuir 2025, 41, 8407−8423

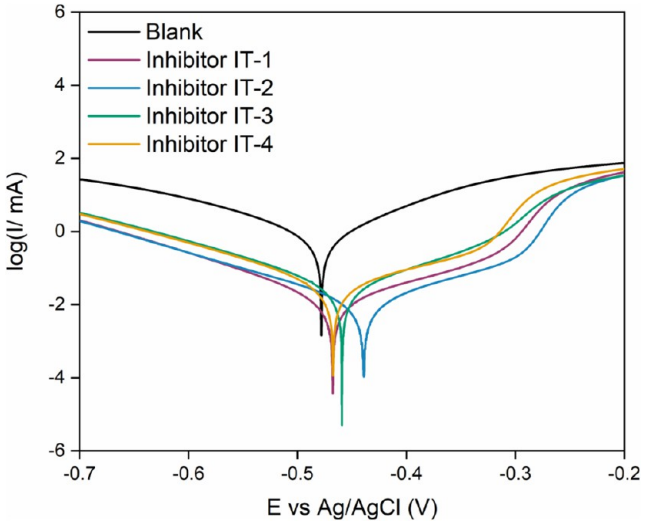

Figure 3. Polarization curves of mild steel coupons in 0.1 M H_2SO_4 in the presence and absence of inhibitors.

thus suppressing corrosion.[68] Furthermore, Table 2 indicates that the E_{corr} values shifted marginally toward anodic potentials in the presence of the inhibitors, with the most significant shift of 38.6 mV observed for inhibitor IT-2. Since this shift falls within the range of ± 85 mV, it can be inferred that the inhibitor molecules protect both cathodic and anodic sites from corrosion, thereby exhibiting mixed behavior.[31]

From the data presented in Table 2, it is evident that the highest current density was observed in the absence of the inhibitor at 486.27 μA cm^{-2}. The corrosion current decreased in the presence of an inhibitor because corrosion involves the transfer of electrons between mild steel and the acidic solution. The inhibitor molecules protect the mild steel by impeding this electron transfer, thereby mitigating corrosion. It is observed that in the presence of inhibitor molecules, the corrosion currents significantly decreased compared to the blank sample, with the lowest corrosion current observed for inhibitor IT-2 at 5.82 μA cm^{-2}. From the $\%\eta_I$ values, it can be inferred that inhibitors IT-1 and IT-2 exhibit better inhibition properties compared to those of inhibitors IT-3 and IT-4. Furthermore, the anodic Tafel slope (β_a) values remain almost constant (except for inhibitor IT-4), suggesting that the inhibitor molecules are adsorbed onto the mild steel surface at the initial stage of its corrosion, blocking surface sites from corrosion without altering the corrosion reaction mechanism.[34]

Table 2. Corrosion Parameters Calculated from Polarization Curves Performed on Mild Steel Coupons with and without Inhibitor Molecules

inhibitor	E_{corr} (mV)	I_{corr} (μA cm^{-2})	β_a (mV/dec)	β_c (mV/dec)	$\%\eta_I$
blank	−478.0	486.27	120.1	147.7	
IT-1	−467.6 (±0.0006)	6.78 (±0.220)	127.4	107.3	98.6 (±0.002)
IT-2	−439.4 (±0.058)	5.82 (±0.010)	127.1	121.8	98.8 (±0.0012)
IT-3	−459.2 (±0.007)	15.51 (±0.071)	121.8	118.4	96.8 (±0.002)
IT-4	−467.2 (±0.002)	18.44 (±0.101)	167.6	123	96.2 (±0.003)

3.3. Gravimetric Analysis. The gravimetric analysis experiments were performed for different concentrations of the inhibitor and at different temperatures. Corrosion parameters such as surface coverage (θ), corrosion rate ($\emptyset$), and inhibition efficiency ($\%\eta_G$) were calculated using eqs 4−6

$$\theta = \frac{w_o - w_i}{w_o} \tag{4}$$

$$\emptyset = \frac{87.6 \times (w_o - w_i)}{D \times A \times t} \tag{5}$$

$$\%\eta_G = \frac{w_o - w_i}{w_o} \times 100 \tag{6}$$

where w_o is weight loss in the absence of inhibitor, w_i is the weight loss in the presence of inhibitor, D is the density of mild steel coupons (g cm^{-3}), A is the surface area of the mild steel coupon (cm^2), and t is the time length of the experiment (h).[69,70]

3.3.1. Langmuir Adsorption Isotherms. We have studied various models to analyze the adsorption characteristics of the corrosion inhibitors on the surface of mild steel (Supporting Information). We found that Langmuir adsorption isotherms provide the best fit when analyzing the adsorption results obtained for the four inhibitors. The adsorption isotherms (Figure 4) were generated by using the concentration of inhibitors (C_{inh}) used during gravimetric experiments and surface coverage (θ) by using the following linear expression (eq 7)[22,71]

$$\frac{C_{inh}}{\theta} = \frac{1}{K_{ads}} + C_{inh} \tag{7}$$

Experiments were performed at five different temperatures (30 to 50 °C), and the intercept obtained from these plots was used to calculate the equilibrium constant of adsorption (K_{ads}). The Gibbs free energy of adsorption (ΔG_{ads}) of the inhibitor molecules was calculated using the K_{ads} values using eq 8

$$\Delta G_{ads} = -RT \times \ln(55.5 \times K_{ads}) \tag{8}$$

where T is the temperature (K), R is the universal gas constant (8.314 J K^{-1} mol^{-1}), and 55.5 is the concentration of water (M) in the solution. These adsorption parameters were interpreted from Figure 4 and are illustrated in the Supporting Information.[72,73]

The obtained equilibrium constants of adsorption K_{ads} were in order of 10^4 across all temperatures (Table 3). These values were on par with previously reported equilibrium constants and were consistent with the strong adsorption of the inhibitors to the surface of the mild steel. IT-2 displayed the highest ΔG_{ads} (−41.44 kJ/mol) at 50 °C, suggesting that inhibitor IT-2 is the most effective in mitigating mild steel corrosion. The order of K_{ads} and ΔG_{ads} is as follows: IT-2 > IT-3 > IT-1 > IT-4. Additionally, ΔG_{ads} ranged between −34.9 and −41.4 kJ/mol. It has been reported that ΔG_{ads} values smaller than −20 kJ/mol indicate physisorption, while values larger than −40 kJ/mol suggest chemisorption. Since most ΔG_{ads} values are close to −40 kJ/mol, it can be inferred that the adsorption of inhibitor molecules on mild steel primarily occurs via chemisorption.[74] This chemisorption likely involves the sharing of π-electrons of inhibitors with the unoccupied 3d orbitals of mild steel.[34,75]

3.3.2. Activation Parameters. The calculation of the activation parameters, namely, activation energy (E_a), activation enthalpy (ΔH_a), and activation entropy (ΔS_a), were performed

https://doi.org/10.1021/acs.langmuir.5c00183
Langmuir 2025, 41, 8407−8423

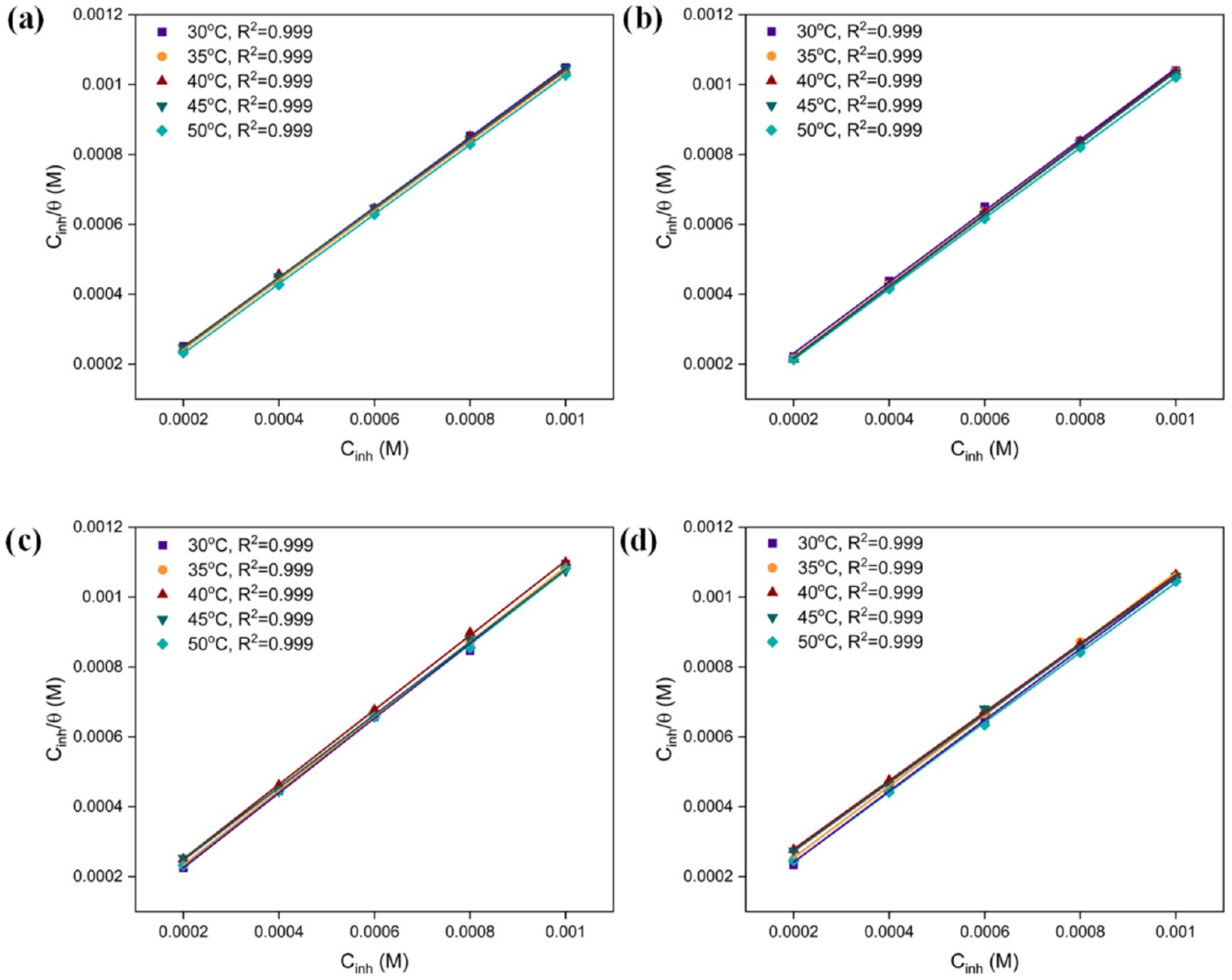

Figure 4. Langmuir adsorption isotherms obtained for (a) inhibitor IT-1, (b) inhibitor IT-2, (c) inhibitor IT-3, and (d) inhibitor IT-4.

Table 3. Adsorption Parameters Calculated from Langmuir Adsorption Isotherms for Inhibitor Molecules at a Temperature of 323 K

inhibitor	K_{ads} x 10^4 (M^{-1})	ΔG_{ads} (kJ/mol)
IT-1	3.16 (±0.250)	−38.63 (±0.022)
IT-2	9.00 (±0.201)	−41.44 (±0.013)
IT-3	4.76 (±0.540)	−39.73 (±0.043)
IT-4	2.38 (±0.028)	−37.86 (±0.002)

using the corrosion rates (Ø) from gravimetric analysis and applying the Arrhenius eq 9 and transition state eq 10 which are presented below

$$\log(Ø) = -\frac{E_a}{2.303 \times RT} + \log \lambda \quad (9)$$

$$\log\left(\frac{Ø}{T}\right) = \log\left(\frac{R}{N_A h}\right) + \left(\frac{\Delta S_a}{2.303 \times R}\right) - \left(\frac{\Delta H_a}{2.303 \times RT}\right) \quad (10)$$

where T is the temperature (K), R is the universal gas constant (8.314 J K^{-1} mol^{-1}), λ is the pre-exponential factor, N_A is Avogadro's number = 6.023 × 10^{23} mol^{-1}, and h is Plank's constant = 6.626 × 10^{-34} m^2 kg s^{-1}.[76,77]

Activation energies were calculated for the adsorption process using the Arrhenius plot (log Ø vs 1000/T) in Figure 5a. E_a values decreased in the presence of inhibitors compared to the blank sample, likely due to the chemisorption of inhibitors by sharing π-electrons with the empty d-orbitals of mild steel (Table 4).[14,34,35] It can also be seen that the values of E_a were in the order of: IT-2 < IT-1 < IT-3 < IT-4. Hence, it can be inferred from the results that IT-1 and IT-2 display a better extent of adsorption on the surface of mild steel in comparison to inhibitors IT-3 and IT-4.

Other activation parameters, such as ΔH_a and ΔS_a, were estimated using the transition state plot (log Ø/T vs 1000/T) in Figure 5b. From Table 4, it can be observed that the ΔH_a values are positive, implying that the corrosion of mild steel in 0.1 M H_2SO_4 is an endothermic process. The decrease in the ΔH_a values in the presence of ITs signifies the mitigation of the corrosion reaction by the inhibitor molecules.[75] The order of ΔH_a values is IT-2 < IT-1 < IT-3 < IT-4. The negative value of ΔS_a for the blank sample results from the mechanism of HER occurring on the mild steel surface. The HER process comprises a sluggish electron transfer from the mild steel substrate, followed by either chemical recombination at lower overpotential levels or electrochemical desorption reactions at higher overpotential levels. The decrease in randomness due to these

https://doi.org/10.1021/acs.langmuir.5c00183
Langmuir 2025, 41, 8407−8423

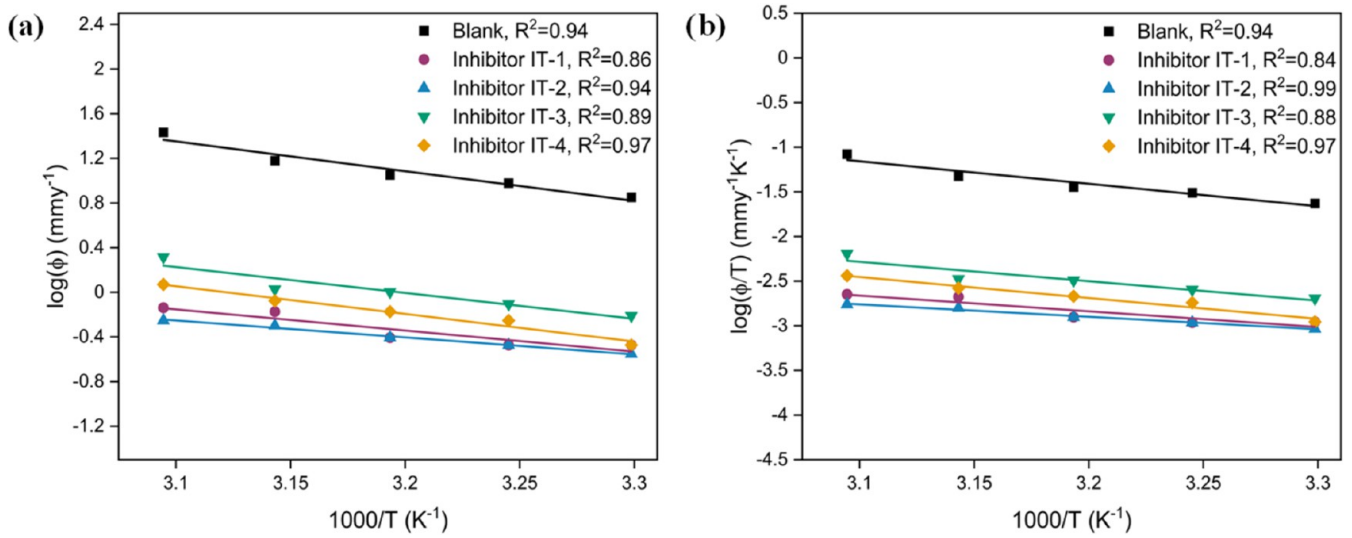

Figure 5. (a) Arrhenius plot (log Ø vs 1000/T) and (b) transition state plot (log Ø/T vs 1000/T) generated from the gravimetric analysis of mild steel coupons in the presence of inhibitors IT-1, IT-2, IT-3, and IT-4.

Table 4. Activation Parameters Estimated from Arrhenius Plots and Transition State Plots

inhibitor	E_a (kJ/mol)	ΔH_a (kJ/mol)	ΔS_a (J/mol·K)
Blank	50.94	48.34	−69.88
IT-1	36.33	33.73	−143.96
IT-2	29.20	26.60	−167.97
IT-3	44.32	41.72	−111.94
IT-4	47.50	44.90	−105.37

intermediate steps results in the negative values of ΔS_a.[34,78,79] In the presence of inhibitor molecules, ΔS_a values were even more negative compared with the blank sample, inferring that the activated states of these processes in the presence of the inhibitor became more organized. As the inhibitor effectively obstructs the cathodic reaction sites to a significant degree, the adsorption of protons on the metal surface and the recombination of surface-adsorbed hydrogen atoms necessitate closer interactions, leading to a more negative ΔS_a value. The order of the ΔS_a values is as follows: IT-2 < IT-1 < IT-3 < IT-4. This indicates that inhibitors IT-2 and IT-1 are better at adsorption onto the mild steel substrate and thus act as better inhibitors.

3.4. Surface Characterization. *3.4.1. SEM and EDS Analysis.* SEM characterizations of the mild steel coupons

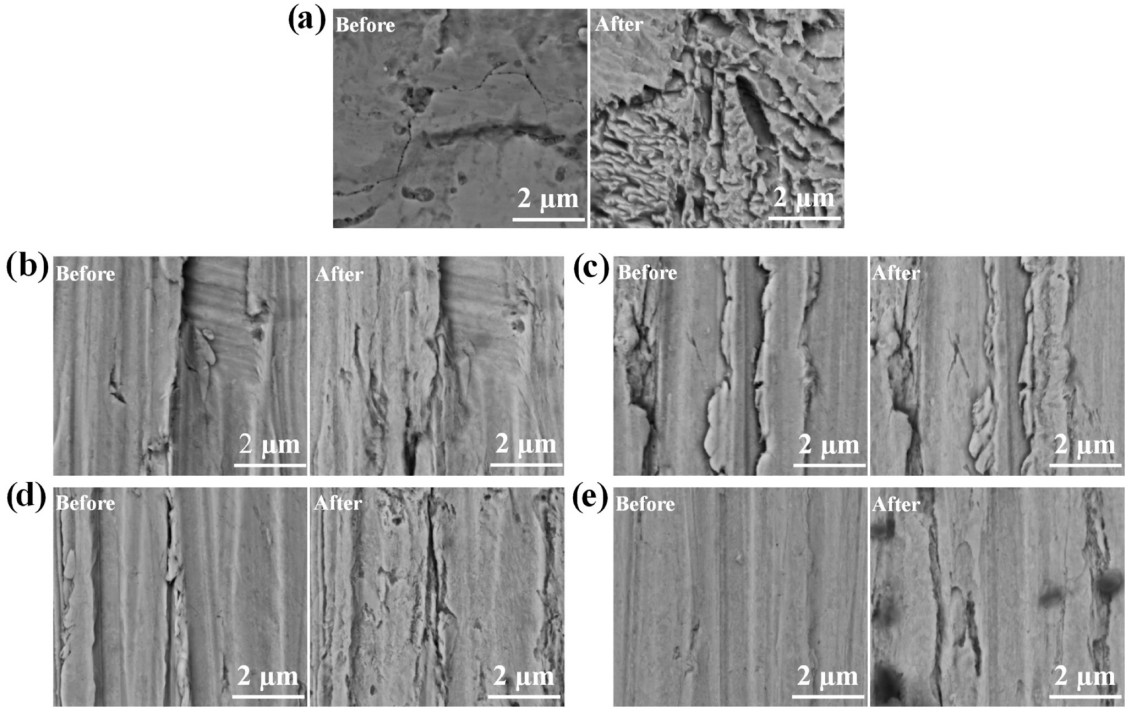

Figure 6. SEM images of mild steel coupons before and after corrosion for 1 h in 0.1 M H_2SO_4: (a) in the absence of inhibitor, (b) in the presence of IT-1, (c) in the presence of IT-2, (d) in the presence of IT-3, and (e) in the presence of IT-4.

https://doi.org/10.1021/acs.langmuir.5c00183
Langmuir 2025, 41, 8407−8423

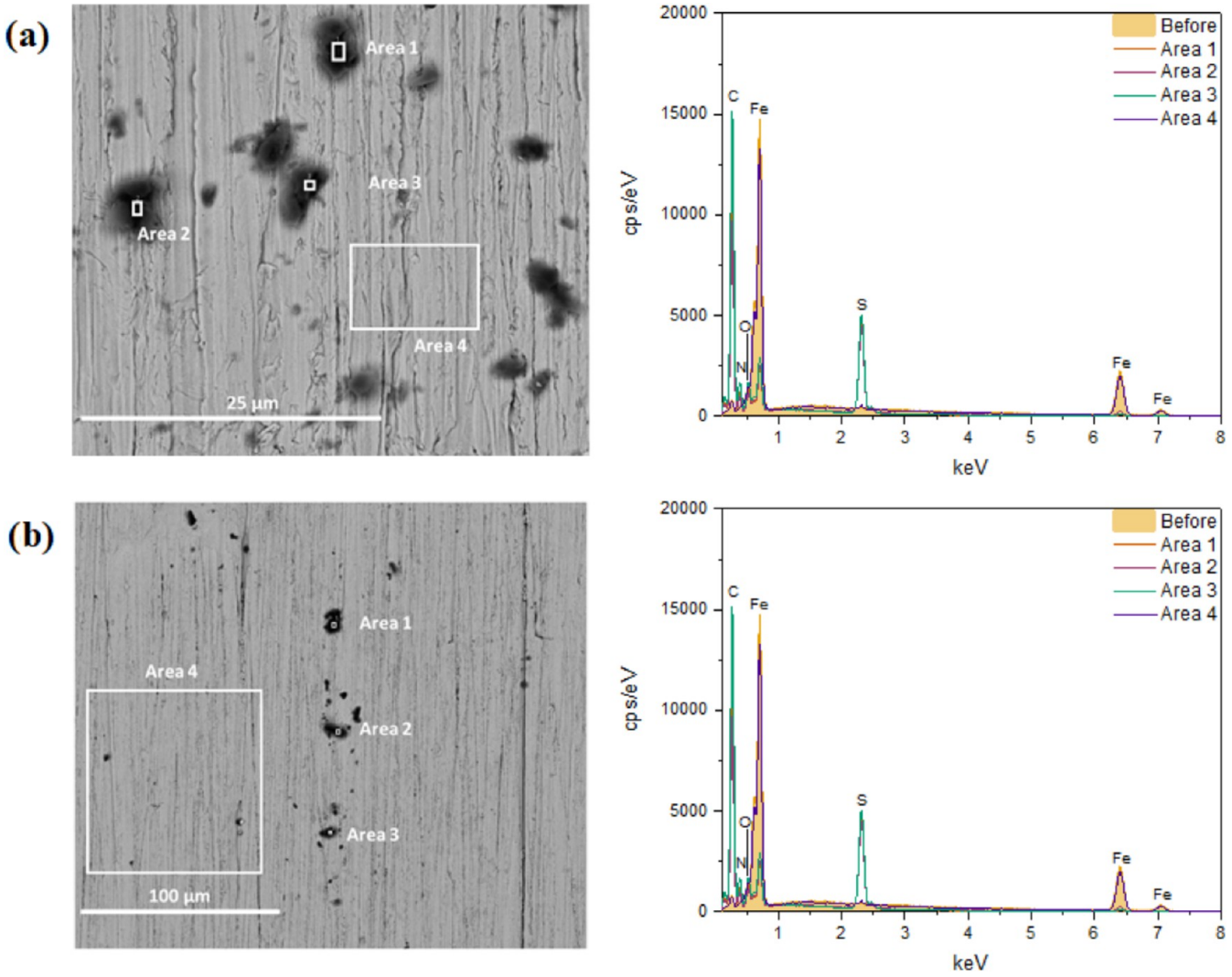

Figure 7. SEM images and selected-area EDS spectra of mild steel coupons corroded in the presence of (a) IT-3 and (b) IT-4. The corresponding elemental compositions are listed in Table 5.

were performed to investigate the effect of the organic inhibitors on surface topology during 1 h corrosion tests in 0.1 M H_2SO_4. To ensure a thorough investigation, SEM images were acquired for the same areas before and after corrosion by taking note of the corresponding axial positions. A rough and unrecognizable surface was observed for the mild steel coupon tested in the absence of an inhibitor (Figure 6a), consistent with the well-documented pitting and partial dissolution that take place during the corrosion of mild steel in acidic media. In contrast, the mild steel's surface was well preserved when 1 mM of corrosion inhibitor was added to the acidic medium, with the same surface features being clearly visible before and after corrosion (Figure 6b–d). These SEM images visually support the electroanalytic and gravimetric results obtained under similar conditions and infer that the inhibitor molecules effectively protect the whole surface of the coupons from corrosion. They also confirm the higher performance of IT-1 and IT-2 as the corresponding images show fewer alterations than those recorded for IT-3 and IT-4.

Interestingly, several dark spots were observed in the backscattered electron images for IT-4 (Figure 6e), suggesting the presence of lower atomic weight elements.[80] These areas were further investigated by EDS to determine the elemental composition of the dark regions and their possible origin. Figure 7a and Table 5 reveal that the spots contain high concentrations of C, N, and S, and a proportionally lower concentration of Fe compared to other areas of the coupon. Considering the analysis depth of EDS (1–2 μm), the elemental analysis suggests that the dark spots correspond to micron-sized deposits of IT-4 on the surface of mild steel. These deposits formed due to the lower solubility of this inhibitor in the acidic solution compared with the other compounds (Figure S5). Similar dark spots, albeit significantly smaller, were also found on the surface of the mild steel coupon treated with IT-3 (Figure 6b). Collectively, these results may explain the deviations between the electroanalytic and gravimetric data noted for IT-3 and IT-4 (vide infra).

3.4.2. XPS Spectroscopy. The mild steel coupons were analyzed by XPS after exposure to corrosion media containing 1 mM of inhibitors. The C, O, N, and Fe spectra were deconvoluted and the corresponding results are presented in the Supporting Information. The C 1s spectra exhibit peaks around 284.4 and 284.8 eV, consistent with the presence of C–C, C═C, and C–H functionalities in the inhibitor molecules.[81] Peaks near 286.2 eV correspond to the C–N linkage within the inhibitor molecules.[82] The presence of thioamide functional groups for all inhibitor molecules gave a peak at 287.5 eV. The

https://doi.org/10.1021/acs.langmuir.5c00183
Langmuir 2025, 41, 8407–8423

Table 5. Elemental Composition in Weight % Calculated from the EDS Analysis of Selected Areas of the Mild Steel Coupons before and after Corrosion in 0.1 M H_2SO_4 in the Presence of Inhibitors IT-3 and IT-4[a]

label	C	N	O	S	Fe	total
inhibitor IT-3						
before corrosion	1.56		0.65		97.70	100
after corrosion area 1	61.85	28.67		9.08	0.41	100
after corrosion area 2	60.40	23.89	0.85	10.27	4.58	100
after corrosion area 3	60.53	25.41		9.16	4.89	100
after corrosion area 4	1.94		1.48	0.74	95.85	100
inhibitor IT-4						
before corrosion	1.24		0.65		98.11	100
after corrosion area 1	49.62	9.56	4.15	14.16	22.51	100
after corrosion area 2	48.88	8.11	3.60	14.12	25.29	100
after corrosion area 3	50.72	11.2	4.11	12.10	21.88	100
after corrosion area 4	1.66		1.02	0.53	96.80	100

[a]Areas 1−3 correspond to spot analyses of the dark regions visible in Figure 7a,b, while Areas 4 correspond to larger regions free of dark features (white rectangles in Figure 7a,b).

peak at 288.7 eV is attributed to the interactions between carbon atoms in the inhibitor molecules and oxygen atoms from the oxidized mild steel surface.

The O 1s spectra revealed peaks around 529.9, 530.9, and 531.6 eV, corresponding to the presence of FeO, FeOOH, and $Fe(OH)_3$, respectively.[83] These findings indicate the presence of oxygenated corrosion products over the protected mild steel substrate, which is consistent with prior reports.[34] The N 1s spectra showed peaks at 398.2 and 399.4 eV, confirming the presence of C═N and −C═S functionalities, respectively, in the inhibitor molecules. The peak around 400.5 eV is characteristic of aromatic-N linkages in the inhibitor molecules, with increased intensity observed for inhibitors IT-3 and IT-4, in good agreement with their molecular structures.[82] Additionally, the N−N linkage in thiosemicarbazone groups gave a peak around 401.8 eV in the N 1s spectra.[84] The Fe 2p spectra appear as a doublet for all inhibitor molecules, with $2p_{3/2}$ observed around 710.8 eV and $2p_{1/2}$ around 724.3 eV. The $2p_{3/2}$ peak is deconvoluted into three distinct peaks: one around 706.5 eV corresponding to the Fe^0 state, one around 710.6 eV corresponding to the Fe^{2+} oxidation state, and one around 714 eV corresponding to the Fe^{3+} oxidation state.[85] These results thereby indicate not only the presence of these inhibitor molecules over the surface of the mild steel coupon but also their attachment to the oxygenated moieties present on the surface of mild steel, thus forming a stronger interaction with the mild steel surface and protecting it from corrosion.

3.4.3. Mass Spectrometry Analysis and Imaging. To quantify the amount of inhibitor molecules adsorbed onto the mild steel coupons, we conducted an LC-MS analysis of the metal samples after 1 h tests in 0.1 M H_2SO_4 containing 1 mM of the desired inhibitor. Solutions containing known concentrations of inhibitors were also prepared and used as external standards for quantification. A list of molecular features was compiled for each inhibitor based on the observed features in the total ion chromatograms (TIC), making sure that the ions were present in abundance both in the standard solutions and in the solutions prepared using the corroded coupons (Supporting Information). As can be seen in Table 6, the performance of the

Table 6. Amounts (in μg) of Indole Thiosemicarbazone Inhibitors Found by LC-MS on the Surface of the Mild Steel Coupons after 1 h Corrosion Tests

inhibitor	adsorbed weight(μg/plate)
IT-1	12.83
IT-2	4.91
IT-3	175.62
IT-4	80.33

IT inhibitors did not scale with the surface concentrations. Relatively low amounts of IT-1 and IT-2, i.e., 5−13 μg per coupon, were sufficient to afford an inhibition efficiency of >98.5%. In contrast, the amounts measured for IT-3 and IT-4 were 1−2 orders of magnitude higher (80−176 μg per coupon). These findings are consistent with the SEM-EDS investigations and the gravimetric results, highlighting that a monolayer of a potent inhibitor is sufficient to offer good protection, while higher concentrations are usually the result of the inhibitor's lower solubility in the aqueous medium and/or the formation of agglomerates on the surface of mild steel. These results also confirm that the performance of an inhibitor is primarily controlled by its electronic structure and the free energy associated with its binding to the surface, not the amount of adsorbed inhibitor.

MALDI-MS was further performed on the coupons to confer spatial resolution to the LC-MS data and visualize the distribution of the inhibitors over the entire metal surface. The ions used for quantification by LC-MS served here to map the organic compounds adsorbed on the surface. Remarkably, the parent ions (M+H+, the protonated and positively charged molecular inhibitors with m/z of 390.10, 394.13, 297.09, and 320.09 for IT-1, IT-2, IT-3, and IT-4, respectively) were evenly distributed across the investigated areas and afforded the strongest signals relative to other ions. The resulting images (Figure 8) confirm that the 4 compounds bind to the entire metal surface, forming a protective layer, and that the aggregates observed by SEM are not the result of poor metal-inhibitor interactions. IT-1 (in pink in Figure 8) showed the most uniform and widespread coverage with virtually no fluctuation in the local concentration. The calculated masses of the detected ions also suggest that the molecular integrity of the compounds is preserved during corrosion tests and that they do not experience significant amounts of acid- or metal-promoted degradation or transformation. This finding is important as it confirms the absence of artifacts and indicates that structure−activity relationships are within reach for this class of inhibitors

3.5. Theoretical Calculations. *3.5.1. HOMO and LUMO Structures of the Indole Thiosemicarbazone Inhibitors.* The geometrical optimization of the inhibitor molecules was performed using DFT calculations to determine the electron-rich sites, i.e., highest occupied molecular orbitals (HOMO), and electron-deficient sites, i.e., lowest unoccupied molecular orbitals (LUMO). These calculations were performed for both the inhibitors in a vacuum and the solvated compounds to understand the effect of solvation on their performance.

The distribution of the HOMO and LUMO orbitals of the molecules in a vacuum was found to vary greatly depending on

https://doi.org/10.1021/acs.langmuir.5c00183
Langmuir 2025, 41, 8407−8423

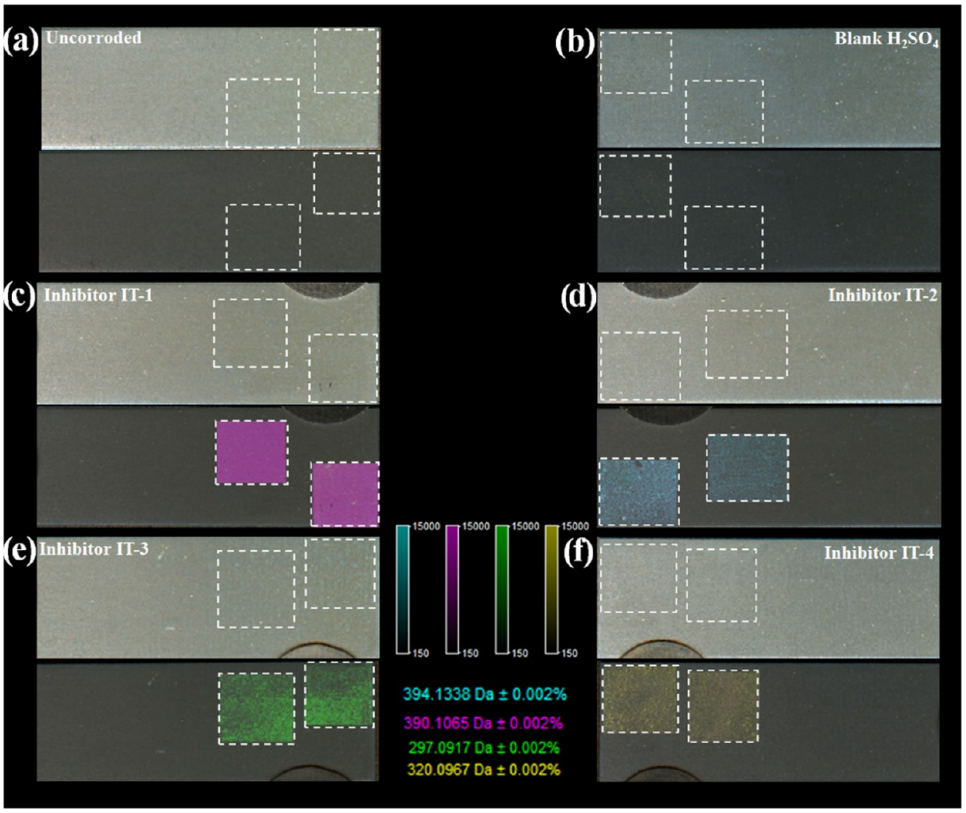

Figure 8. MALDI-MS mapping of mild steel coupons. An optical image (top) and the selected-area maps computed using the signal of the most abundant ions (bottom) are provided for each of the six samples: (a) pristine mild steel coupon, (b) coupon exposed 0.1 M H_2SO_4 in the absence of inhibitor, and samples exposed to 0.1 M H_2SO_4 containing 1 mM of (c) IT-1, (d) IT-2, (e) IT-3, and (f) IT-4.

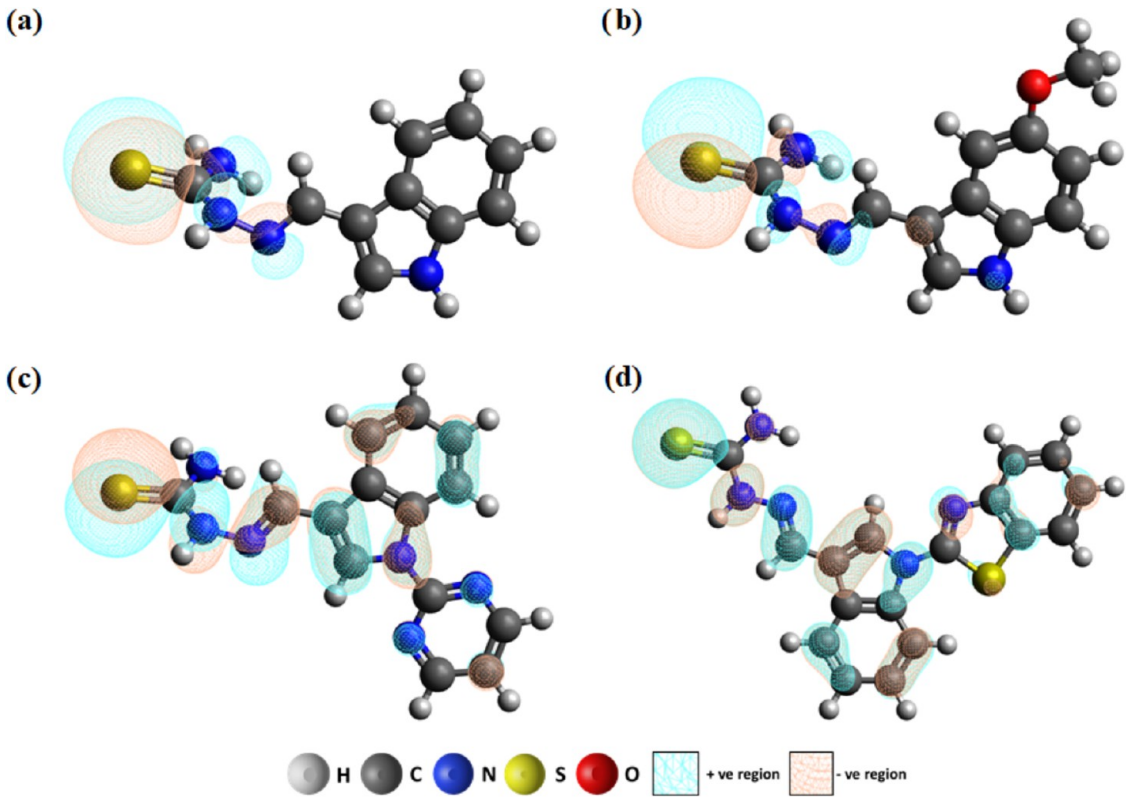

Figure 9. HOMO structure for vacuum of inhibitor molecules (a) IT-1, (b) IT-2, (c) IT-3, and (d) IT-4, computed through DFT-B3LYP/6-31G using Gaussian 16 program.

https://doi.org/10.1021/acs.langmuir.5c00183
Langmuir 2025, 41, 8407−8423

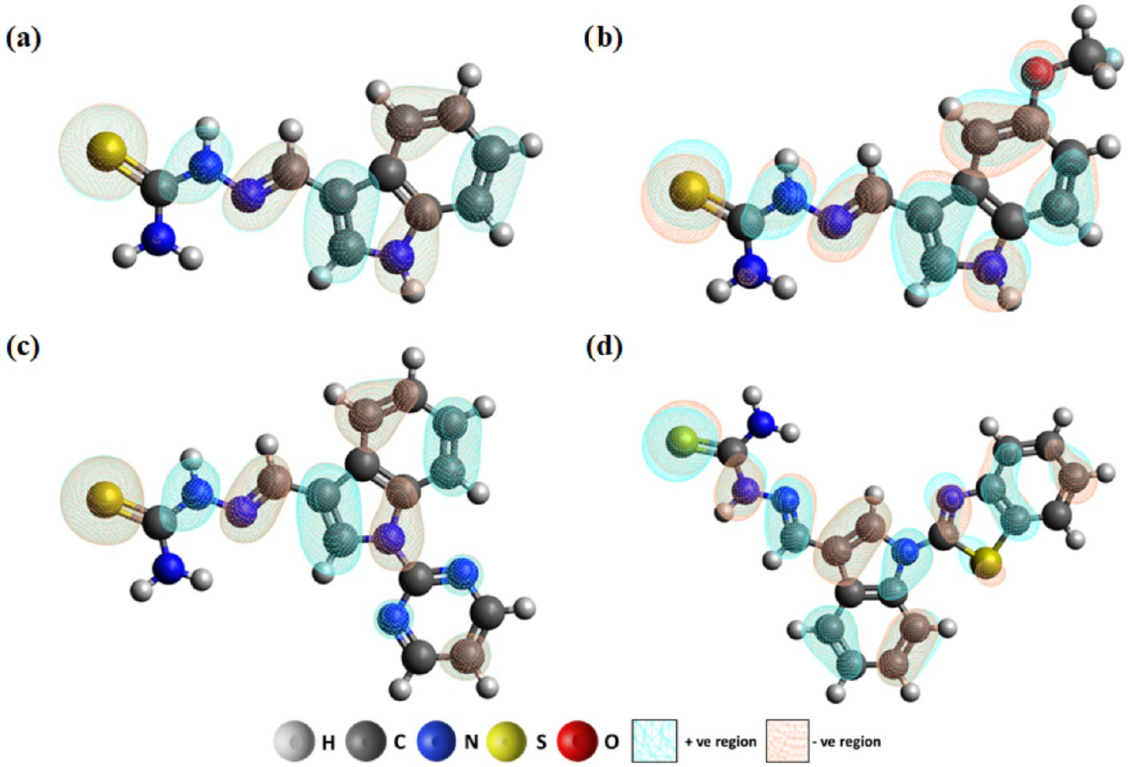

Figure 10. HOMO structure for solvation of inhibitor molecules (a) IT-1, (b) IT-2, (c) IT-3, and (d) IT-4, computed through DFT-B3LYP/6-31G using Gaussian 16 program.

Table 7. Molecular Reactivity Parameters Obtained from DFT Calculations

inhibitor	E_H (eV)	E_L (eV)	ΔE (eV)	χ (eV)	γ (eV)	σ(eV^{-1})	ΔN
IT-1 vacuum	−5.391	−1.456	3.935	3.423	1.968	0.508	0.909
IT-1 solvated	−4.939	−0.814	4.125	2.876	2.062	0.485	1.000
IT-2 vacuum	−5.285	−1.381	3.904	3.333	1.952	0.512	0.939
IT-2 solvated	−4.824	−0.768	4.056	2.796	2.028	0.493	1.036
IT-3 vacuum	−5.435	−1.822	3.613	3.629	1.806	0.554	0.933
IT-3 solvated	−5.025	−1.204	3.114	3.114	1.910	0.523	1.017
IT-4 vacuum	−5.428	−1.832	3.630	3.630	1.798	0.556	0.937
IT-4 solvated	−5.010	−1.226	3.118	3.118	1.892	0.529	1.026

the nature of the side groups despite the four inhibitors sharing the same indole thiosemicarbazone platform structure (Figure 9). These differences highlight the importance of side groups on the electronic structure of the whole molecule, suggesting that the performance of an organic corrosion inhibitor can be tailored to a great extent through simple chemical derivatization. These results also highlight that the electronic structure of an organic corrosion inhibitor cannot simply be described as the cumulative contribution of the individual building blocks that form the molecule. As such, the presence of multiple electron-rich heteroatoms (N, S, and O) is not a guarantee of high corrosion inhibition. Instead, these results suggest that DFT calculations are required to explain and predict their performance.

Our calculations also reveal the important role played by the solvent in the electronic structure and performance of these compounds (Figure 10). While the HOMO of IT-1 and IT-2 was localized in the thioamide part of the inhibitors when computed in a vacuum, the orbital was also distributed in the indole part of the molecules upon solvation. Since HOMO orbitals are electron-rich, the redistribution of the HOMO for IT-1 and IT-2 indicates an enhanced electron donation capability of these inhibitor molecules under solvated conditions, where corrosion typically occurs.[86,87] Interestingly, we observed minimal changes in the HOMO and LUMO distribution upon solvation for inhibitors IT-3 and IT-4.

The simulated Mulliken charges for each of the atoms of the four inhibitors are presented in the Supporting Information. As anticipated, the heteroatoms carry negative charges that facilitate the inhibitors' interactions with the electron-deficient metal surface.[34,88] Interestingly, some of the charges became more pronounced for the solvated molecules, further highlighting the role of the solvent in their electronic structure and adsorption properties.

3.5.2. Molecular Reactivity Calculations. The reactivity of organic corrosion inhibitors can be further estimated from the position of HOMO (E_H) and LUMO (E_L) orbitals, global hardness (γ), softness (σ), electronegativity (χ), and fraction of electrons transferred to the surface of the metal (ΔN). These parameters were calculated for both the inhibitors in a vacuum and the solvated molecules using eqs 11−15

$$\Delta E = E_L - E_H \tag{11}$$

https://doi.org/10.1021/acs.langmuir.5c00183
Langmuir 2025, 41, 8407−8423

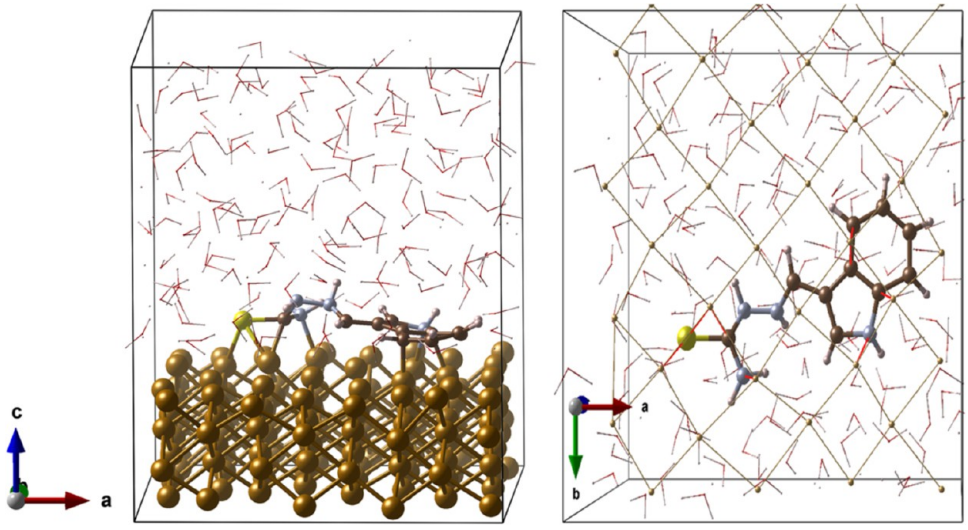

Figure 11. Adsorption of inhibitor IT-1 on a Fe(110) surface in liquid water (left: side view; right: top view). Atom legend: yellow: S, brown: C, white: H, blue: N, gold: Fe. The gold mesh represents the Fe(110) surface, while the water was presented as red-white wires.

$$\chi = -\frac{E_L + E_H}{2} \tag{12}$$

$$\gamma = \frac{E_L - E_H}{2} \tag{13}$$

$$\sigma = 1/\gamma \tag{14}$$

$$\Delta N = \frac{\chi_{Fe} - \chi_{inh}}{2\,\gamma_{inh}};\ \chi_{Fe} = 7.0\ \text{eV} \tag{15}$$

The reactivity parameters calculated from the above equations are listed in Table 7. E_H values indicate the electron donation ability of the inhibitor molecule to the empty d-orbitals of metal atoms while E_L values indicate their electron back acceptance ability. It has been previously established that small values (less negative) for both E_H and E_L favor the strong adsorption of organic corrosion inhibitors to the metal surface.[78] Likewise, a lower ΔE, defined as the energy difference between HOMO and LUMO orbitals, is an indicator of chemical reactivity, which can play a role in inhibitors that protect metals through sacrificial oxidation. As can be seen in Table 7, IT-1 and IT-2 have E_H and E_L energies 0.1−0.2 lower than those of IT-3 and IT-4. The solvent further lowers their energies by 0.4−0.6 eV, in good agreement with the changes in the molecular orbitals and the stronger binding anticipated from Figures 9 and 10. Interestingly, the trend observed for ΔE values is inconsistent with the inhibition efficiencies observed experimentally. This discrepancy has been reported by other research groups and likely indicates that the IT inhibitors adsorb and form a protective layer on the metal rather than acting as a sacrificial redox compound.[14,33,89,]

Other performance indicators, namely, electronegativity and the fraction of electrons transferred with the metal surface, are also fully consistent with the better performance of IT-1 and IT-2. Specifically, low electronegativity favors the transfer of electrons from the organic compound to the metal (χ_{Fe} = 7.0 eV) until their chemical potentials come into equilibrium.[91] The ∼0.3 eV lower values for IT-1 and IT-2 compared with IT-3 and IT-4 again support the stronger adsorption of the former. In addition, ΔN values lower than 3.6 imply a high tendency of the inhibitors to donate electrons to the mild steel substrate. Here, all of the ΔN values were found to range between 0.9 and 1.0, indicating a similar adsorption process by electron donation for the four compounds.[92,93]

3.5.3. Ab Initio Molecular Dynamics (AIMD) Simulations. AIMD simulations were performed to better understand the role played by the solvent at an experimentally relevant temperature of 300 K. The simulations were performed for IT-1 in the presence of a water monolayer and bulk water to study (i) how the inhibitor displaces the water molecules near the surface during adsorption and (ii) how water alters its electronic structure and binding energy. All simulations were performed for Fe (110) as a representative surface for mild steel.[94−96]

In the presence of a water monolayer, IT-1 was found to physisorb on the water molecules through interactions between the indole fragment of the inhibitor and the hydrogen atoms of H_2O. However, spontaneous chemisorption occurred in the presence of bulk water (Figure 11). These results further highlight that instead of impeding the diffusion and adsorption of the inhibitors, water molecules actually facilitate the chemisorption of the solvated compounds by promoting their electronic structure and binding affinity.

4. CONCLUSIONS

In conclusion, the biobased corrosion inhibitors developed in this work demonstrate exceptional efficacy in mitigating mild steel corrosion in acidic environments. The findings from electrochemical impedance spectroscopy and polarization curve analyses indicated that they not only exhibit high corrosion inhibition efficiencies but also protect both cathodic and anodic sites from corrosion. Further, gravimetric analysis revealed that IT inhibitors follow the Langmuir model of adsorption, and the values of ΔG_{ads} (close to −40 kJ/mol) revealed they are chemisorbed to the surface of mild steel. From both electrochemical and gravimetric analyses, it can be inferred that inhibitors IT-1 and IT-2 have superior performance in mitigating corrosion in comparison to inhibitors IT-3 and IT-4.

SEM images of mild steel coupons before and after corrosion confirmed a significant reduction in the degree of corrosion in the presence of IT inhibitors. Additionally, inhibitors IT-3 and IT-4 were found to form deposits on the mild steel surface, which may account for the deviations observed between the

https://doi.org/10.1021/acs.langmuir.5c00183
Langmuir 2025, 41, 8407−8423

electrochemical and gravimetric analyses. LC-MS and MALDI-MS confirmed that the inhibitor molecules covered and protected the whole mild steel surface with IT-2 offering the highest protection at a surface concentration as low as 0.7 $\mu g\ cm^{-2}$. Moreover, DFT calculations provided valuable insights into the HOMO and LUMO positions on the molecules, revealing, in particular, the role of side groups on the electronic structure of the indole thiosemicarbazone platform. Other computed reactivity parameters aligned well with experimental observations. Overall, both experimental and theoretical results affirm that inhibitors IT-1 and IT-2 possess better corrosion inhibition capabilities compared with inhibitors IT-3 and IT-4 that can be traced back to their electronic structure. Finally, DFT and AIMD results showed that solvation played an important role in enhancing the electronic properties and driving their chemisorption.

■ ASSOCIATED CONTENT

Supporting Information

The Supporting Information is available free of charge at https://pubs.acs.org/doi/10.1021/acs.langmuir.5c00183.

Additional experimental procedures, adsorption isotherms, adsorption parameters, photos of solutions, XPS spectra, computed molecular structures, Mulliken charges, and parameters calculated from the fitting of the Nyquist plots (PDF)

■ AUTHOR INFORMATION

Corresponding Authors

George A. Kraus − *Department of Chemistry, Iowa State University, Ames, Iowa 50011, United States;* orcid.org/0000-0002-3037-8413; Email: gakraus@iastate.edu

Jean-Philippe Tessonnier − *Department of Chemical and Biological Engineering, Iowa State University, Ames, Iowa 50011, United States;* orcid.org/0000-0001-9035-634X; Email: tesso@iastate.edu

Authors

A. K. S. Koushik − *Department of Chemical and Biological Engineering, Iowa State University, Ames, Iowa 50011, United States*

Demetrius Finley − *Department of Chemistry, Iowa State University, Ames, Iowa 50011, United States*

Nadia N. Intan − *Department of Chemical Engineering, University of Washington, Seattle, Washington 98195, United States; Physical Sciences Division, Physical & Computational Sciences Directorate, Pacific Northwest National Laboratory, Richland, Washington 99352, United States;* orcid.org/0000-0003-1967-178X

Lucas J. Showman − *W.M. Keck Metabolomics Research Laboratory, Iowa State University, Ames, Iowa 50010, United States*

Kyle Podolak − *Department of Chemistry, Iowa State University, Ames, Iowa 50011, United States*

Zachery Crandall − *Department of Chemistry, Iowa State University, Ames, Iowa 50011, United States; Chemical and Biological Sciences, Ames National Laboratory, Ames, Iowa 50011, United States*

Theresa L. Windus − *Department of Chemistry, Iowa State University, Ames, Iowa 50011, United States; Chemical and Biological Sciences, Ames National Laboratory, Ames, Iowa 50011, United States;* orcid.org/0000-0001-6065-3167

Jim Pfaendtner − *Department of Chemical & Biomolecular Engineering, North Carolina State University, Raleigh, North Carolina 27695, United States;* orcid.org/0000-0001-6727-2957

Siegfried R. Waldvogel − *Department of Electrosynthesis, Max-Planck-Institute for Chemical Energy Conversion, Mülheim an der Ruhr 45470, Germany*

Complete contact information is available at: https://pubs.acs.org/10.1021/acs.langmuir.5c00183

Author Contributions

◆These authors contributed equally to the present work. A.K.S.K.: Conceptualization, methodology, investigation, data curation, formal analysis, visualization, validation, writing—original draft, writing—review and editing. D.F.: Conceptualization, methodology, investigation, writing—original draft. N.N.I.: Methodology, investigation, formal analysis, visualization, writing—original draft. L.J.S.: Methodology, investigation, data curation, formal analysis, visualization, writing—original draft. K.P.: Methodology, investigation. Z.C.: Methodology, investigation, data curation, formal analysis, writing—original draft. T.L.W.: Methodology, formal analysis, writing—review and editing. J.P.: Methodology, funding acquisition. S.R.W.: Methodology. G.A.K.: Conceptualization, supervision, funding acquisition, writing—original draft, writing—review and editing. J.-P.T.: Conceptualization, supervision, funding acquisition, writing—original draft, writing—review and editing.

Notes

The authors declare no competing financial interest.

■ ACKNOWLEDGMENTS

This research was partially supported by the U.S. Department of Energy's Office of Energy Efficiency and Renewable Energy (EERE) under the Bioenergy Technologies Office Award Number DE-EE0008492, and by the National Science Foundation under grant number CBET-2140342. N.N.I. also acknowledges the support provided by Pacific Northwest National Laboratory, under the U.S. Department of Energy, Office of Science, Office of Basic Energy Sciences, Division of Chemical Sciences, Geosciences, and Biosciences Division, Condensed Phase and Interfacial Molecular Science program, FWP 16249. Pacific Northwest National Laboratory is a multiprogram national laboratory operated for the DOE by Batelle Memorial Institute under Contract DE-AC05-76RL0-1630. Computational resources for this work were provided by the Hyak supercomputer system of the University of Washington and the National Energy Research Scientific Computing Center (NERSC), a U.S. Department of Energy Office of Science User Facility operated under Contract No. DE-AC02-05CH11231. Z.C. and T.L.W. thank support from the U.S. Department of Energy, Office of Science, Basic Energy Sciences, Chemical Sciences, Geosciences, and Biosciences Division, Computational and Theoretical Chemistry program through the Ames National Laboratory. The Ames National Laboratory is operated for the U.S. Department of Energy by Iowa State University under Contract No. DEAC02-07CH11358.

REFERENCES

(1) Finšgar, M.; Jackson, J. Application of Corrosion Inhibitors for Steels in Acidic Media for the Oil and Gas Industry: A Review. *Corros. Sci.* **2014**, *86*, 17−41.

(2) Makhlouf, A. S.; H Herrera, V.; Muñoz, E. Chapter 6 - Corrosion and Protection of the Metallic Structures in the Petroleum Industry Due to Corrosion and the Techniques for Protection. In *Handbook of Materials Failure Analysis*; Makhlouf, A. S.; H Aliofkhazraei, M., Eds.; Butterworth-Heinemann, 2018; pp 107−122 DOI: 10.1016/B978-0-08-101928-3.00006-9.

(3) Dohare, P.; Quraishi, M. A.; Obot, I. B. A Combined Electrochemical and Theoretical Study of Pyridine-Based Schiff Bases as Novel Corrosion Inhibitors for Mild Steel in Hydrochloric Acid Medium. *J. Chem. Sci.* **2018**, *130*, No. 8.

(4) Wang, D.; Li, Y.; Chang, T.; et al. Experimental and Theoretical Studies of Chitosan Derivatives as Green Corrosion Inhibitor for Oil and Gas Well Acid Acidizing. *Colloids Surf., A* **2021**, *628*, No. 127308.

(5) Xu, B.; Yang, W.; Liu, Y.; et al. Experimental and Theoretical Evaluation of Two Pyridinecarboxaldehyde Thiosemicarbazone Compounds as Corrosion Inhibitors for Mild Steel in Hydrochloric Acid Solution. *Corros. Sci.* **2014**, *78*, 260−268.

(6) Noor, E. A.; Al-Moubaraki, A. H. Corrosion Behavior of Mild Steel in Hydrochloric Acid Solutions. *Int. J. Electrochem. Sci.* **2008**, *3*, 806−818.

(7) Bahrami, M. J.; Hosseini, S. M. A.; Pilvar, P. Experimental and Theoretical Investigation of Organic Compounds as Inhibitors for Mild Steel Corrosion in Sulfuric Acid Medium. *Corros. Sci.* **2010**, *52*, 2793−2803.

(8) Kendig, M. W.; Buchheit, R. G. Corrosion Inhibition of Aluminum and Aluminum Alloys by Soluble Chromates, Chromate Coatings, and Chromate-Free Coatings. *Corrosion* **2003**, *59*, 379−400.

(9) Zehra, S.; Mobin, M.; Aslam, J. Chapter 13 - Chromates as Corrosion Inhibitors. In *Inorganic Anticorrosive Materials*; Verma, C.; Aslam, J.; Hussain, C. M., Eds.; Elsevier, 2022; pp 251−268 DOI: 10.1016/B978-0-323-90410-0.00014-3.

(10) Vukasovich, M. S.; Farr, J. P. G. Molybdate in Corrosion Inhibition—a Review. *Polyhedron* **1986**, *5*, 551−559.

(11) Costa, M.; Klein, C. B. Toxicity and Carcinogenicity of Chromium Compounds in Humans. *Crit. Rev. Toxicol.* **2006**, *36*, 155−163.

(12) Mamyrbaev, A. A.; Dzharkenov, T. A.; Imangazina, Z. A.; et al. Mutagenic and Carcinogenic Actions of Chromium and Its Compounds. *Environ. Health Prev. Med.* **2015**, *20*, 159−167.

(13) Holmes, A. L.; Wise, S. S.; Wise, J. P. Carcinogenicity of Hexavalent Chromium. *Indian J. Med. Res.* **2008**, *128*, 353−372.

(14) Zhang, Q. H.; Hou, B. S.; Zhang, G. A. Inhibitive and Adsorption Behavior of Thiadiazole Derivatives on Carbon Steel Corrosion in CO_2-Saturated Oilfield Produced Water: Effect of Substituent Group on Efficiency. *J. Colloid Interface Sci.* **2020**, *572*, 91−106.

(15) Talebian, M.; Raeissi, K.; Atapour, M.; et al. Inhibitive Effect of Sodium (E)-4-(4-Nitrobenzylideneamino)Benzoate on the Corrosion of Some Metals in Sodium Chloride Solution. *Appl. Surf. Sci.* **2018**, *447*, 852−865.

(16) Ba-Shammakh, M. S. *Electropolymerization of Pyrrole on Mild Steel for Corrosion Protection*; M.S., King Fahd University of Petroleum and Minerals (Saudi Arabia): Saudi Arabia, 2002.

(17) Verma, C.; Ebenso, E. E.; Bahadur, I.; et al. 5-(Phenylthio)-3h-Pyrrole-4-Carbonitriles as Effective Corrosion Inhibitors for Mild Steel in 1M HCl: Experimental and Theoretical Investigation. *J. Mol. Liq.* **2015**, *212*, 209−218.

(18) Zarrouk, A.; Hammouti, B.; Lakhlifi, T.; et al. New 1h-Pyrrole-2,5-Dione Derivatives as Efficient Organic Inhibitors of Carbon Steel Corrosion in Hydrochloric Acid Medium: Electrochemical, XPS and DFT Studies. *Corros. Sci.* **2015**, *90*, 572−584.

(19) Pavithra, M. K.; Venkatesha, T. V.; Punith Kumar, M. K.; et al. Inhibition of Mild Steel Corrosion by Rabeprazole Sulfide. *Corros. Sci.* **2012**, *60*, 104−111.

(20) Verma, C.; Olasunkanmi, L. O.; Quadri, T. W.; et al. Gravimetric, Electrochemical, Surface Morphology, DFT, and Monte Carlo Simulation Studies on Three N-Substituted 2-Aminopyridine Derivatives as Corrosion Inhibitors of Mild Steel in Acidic Medium. *J. Phys. Chem. C* **2018**, *122*, 11870−11882.

(21) Zheng, X.; Zhang, S.; Gong, M.; et al. Experimental and Theoretical Study on the Corrosion Inhibition of Mild Steel by 1-Octyl-3-Methylimidazolium L-Prolinate in Sulfuric Acid Solution. *Ind. Eng. Chem. Res.* **2014**, *53*, 16349−16358.

(22) Zhou, T.; Yuan, J.; Zhang, Z.; et al. The Comparison of Imidazolium Gemini Surfactant [C14−4-C14im]Br2 and Its Corresponding Monomer as Corrosion Inhibitors for A3 Carbon Steel in Hydrochloric Acid Solutions: Experimental and Quantum Chemical Studies. *Colloids Surf., A* **2019**, *575*, 57−65.

(23) Obot, I. B.; Umoren, S. A.; Gasem, Z. M.; et al. Theoretical Prediction and Electrochemical Evaluation of Vinylimidazole and Allylimidazole as Corrosion Inhibitors for Mild Steel in 1M HCl. *J. Ind. Eng. Chem.* **2015**, *21*, 1328−1339.

(24) Zhou, Y.; Guo, L.; Zhang, S.; et al. Corrosion Control of Mild Steel in 0.1 m H_2SO_4 Solution by Benzimidazole and Its Derivatives: An Experimental and Theoretical Study. *RSC Adv.* **2017**, *7*, 23961−23969.

(25) Mehmeti, V. V.; Berisha, A. R. Corrosion Study of Mild Steel in Aqueous Sulfuric Acid Solution Using 4-Methyl-4h-1,2,4-Triazole-3-Thiol and 2-Mercaptonicotinic Acid—an Experimental and Theoretical Study. *Front. Chem.* **2017**, *5*, No. 61.

(26) El Bakri, Y.; Guo, L.; Anouar, E. H.; et al. Electrochemical, DFT and MD Simulation of Newly Synthesized Triazolotriazepine Derivatives as Corrosion Inhibitors for Carbon Steel in 1 M Hcl. *J. Mol. Liq.* **2019**, *274*, 759−769.

(27) Paul, P. K.; Yadav, M. Investigation on Corrosion Inhibition and Adsorption Mechanism of Triazine-Thiourea Derivatives at Mild Steel/HCl Solution Interface: Electrochemical, XPS, DFT and Monte Carlo Simulation Approach. *J. Electroanal. Chem.* **2020**, *877*, No. 114599.

(28) Rbaa, M.; Abousalem, A. S.; Rouifi, Z.; et al. Synthesis, Antibacterial Study and Corrosion Inhibition Potential of Newly Synthesis Oxathiolan and Triazole Derivatives of 8-Hydroxyquinoline: Experimental and Theoretical Approach. *Surf. Interfaces* **2020**, *19*, No. 100468.

(29) Khaled, K. F.; Amin, M. A. Corrosion Monitoring of Mild Steel in Sulphuric Acid Solutions in Presence of Some Thiazole Derivatives − Molecular Dynamics, Chemical and Electrochemical Studies. *Corros. Sci.* **2009**, *51*, 1964−1975.

(30) Gong, W.; Xu, B.; Yin, X.; et al. Halogen-Substituted Thiazole Derivatives as Corrosion Inhibitors for Mild Steel in 0.5 M Sulfuric Acid at High Temperature. *J. Taiwan Inst. Chem. Eng.* **2019**, *97*, 466−479.

(31) Yang, Z.; Zhan, F.; Pan, Y.; et al. Structure of a Novel Benzyl Quinolinium Chloride Derivative and Its Effective Corrosion Inhibition in 15wt.% Hydrochloric Acid. *Corros. Sci.* **2015**, *99*, 281−294.

(32) Kumar, C. B. P.; Prashanth, M. K.; Mohana, K. N.; et al. Protection of Mild Steel Corrosion by Three New Quinazoline Derivatives: Experimental and DFT Studies. *Surf. Interfaces* **2020**, *18*, No. 100446.

(33) Errahmany, N.; Rbaa, M.; Abousalem, A. S.; et al. Experimental, DFT Calculations and MC Simulations Concept of Novel Quinazolinone Derivatives as Corrosion Inhibitor for Mild Steel in 1.0 M HCl Medium. *J. Mol. Liq.* **2020**, *312*, No. 113413.

(34) Sarkar, T. K.; Yadav, M.; Obot, I. B. Mechanistic Evaluation of Adsorption and Corrosion Inhibition Capabilities of Novel Indoline Compounds for Oil Well/Tubing Steel in 15% HCl. *Chem. Eng. J.* **2022**, *431*, No. 133481.

(35) de Souza, F. S.; Spinelli, A. Caffeic Acid as a Green Corrosion Inhibitor for Mild Steel. *Corros. Sci.* **2009**, *51*, 642−649.

(36) Aslam, R.; Serdaroglu, G.; Zehra, S.; et al. Corrosion Inhibition of Steel Using Different Families of Organic Compounds: Past and Present Progress. *J. Mol. Liq.* **2022**, *348*, No. 118373.

(37) Abd El-Lateef, H. M.; Soliman, K. A.; Tantawy, A. H. Novel Synthesized Schiff Base-Based Cationic Gemini Surfactants: Electrochemical Investigation, Theoretical Modeling and Applicability as Biodegradable Inhibitors for Mild Steel against Acidic Corrosion. *J. Mol. Liq.* **2017**, *232*, 478−498.

https://doi.org/10.1021/acs.langmuir.5c00183
Langmuir 2025, 41, 8407−8423

(38) Kosuge, T.; Heskett, M. G.; Wilson, E. E. Microbial Synthesis and Degradation of Indole-3-Acetic Acid: I. The Conversion of L-Tryptophan to Indole-3-Acetamide by an Enzyme System from Pseudomonas Savastanoi. *J. Biol. Chem.* **1966**, *241*, 3738−3744.
(39) El-Sawy, E.; Abo-Salem, H.; Mandour, A. 1h-Indole-3-Carboxaldehyde: Synthesis and Reactions. *Egypt. J. Chem.* **2017**, *60*, 723−751.
(40) Lira, A. B.; Parrilha, G. L.; Dias, G. T.; et al. Evaluation of Toxicity and Oxidative Stress of 2-Acetylpyridine-N(4)-Orthochlorophenyl Thiosemicarbazone. *Oxid. Med. Cell. Longevity* **2022**, *2022*, No. 4101095.
(41) Xia, G.; Jiang, X.; Zhou, L.; et al. Synergic Effect of Methyl Acrylate and N-Cetylpyridinium Bromide in N-Cetyl-3-(2-Methoxycarbonylvinyl)Pyridinium Bromide Molecule for X70 Steel Protection. *Corros. Sci.* **2015**, *94*, 224−236.
(42) Chen, Y.; Liu, Y.; Allegood, J.et al. Imaging Maldi Mass Spectrometry of Sphingolipids Using an Oscillating Capillary Nebulizer Matrix Application System. In *Mass Spectrometry Imaging: Principles and Protocols*; Rubakhin, S. S.; Sweedler, J. V., Eds.; Humana Press: Totowa, NJ, 2010; pp 131−146 DOI: 10.1007/978-1-60761-746-4_7.
(43) Frisch, M. J.; Trucks, G. W.; Schlegel, H. B.et al. *Gaussian 16*, revision C.01; Gaussian Inc.: Wallingford, CT, 2016.
(44) Becke, A. Density-Functional Thermochemistry. Iii. The Role of Exact Exchange. *J. Chem. Phys.* **1993**, *98*, No. 5648.
(45) Lee, C.; Yang, W.; Parr, R. G. Development of the Colle-Salvetti Correlation-Energy Formula into a Functional of the Electron Density. *Phys. Rev. B* **1988**, *37*, 785−789.
(46) Rassolov, V. A.; Pople, J. A.; Ratner, M. A.; et al. 6−31g* Basis Set for Atoms K through Zn. *J. Chem. Phys.* **1998**, *109*, 1223−1229.
(47) Miertuš, S.; Scrocco, E.; Tomasi, J. Electrostatic Interaction of a Solute with a Continuum. A Direct Utilizaion of Ab Initio Molecular Potentials for the Prevision of Solvent Effects. *Chem. Phys.* **1981**, *55*, 117−129.
(48) Miertuš, S.; Tomasi, J. Approximate Evaluations of the Electrostatic Free Energy and Internal Energy Changes in Solution Processes. *Chem. Phys.* **1982**, *65*, 239−245.
(49) Pascual-ahuir, J. L.; Silla, E.; Tuñon, I. Gepol: An Improved Description of Molecular Surfaces. Iii. A New Algorithm for the Computation of a Solvent-Excluding Surface. *J. Comput. Chem.* **1994**, *15*, 1127−1138.
(50) Kirkwood, J. G. Theory of Solutions of Molecules Containing Widely Separated Charges with Special Application to Zwitterions. *J. Chem. Phys.* **1934**, *2*, 351−361.
(51) Onsager, L. Electric Moments of Molecules in Liquids. *J. Am. Chem. Soc.* **1936**, *58*, 1486−1493.
(52) Wong, M. W.; Frisch, M. J.; Wiberg, K. B. Solvent Effects. 1. The Mediation of Electrostatic Effects by Solvents. *J. Am. Chem. Soc.* **1991**, *113*, 4776−4782.
(53) Wong, M. W.; Wiberg, K. B.; Frisch, M. Hartree−Fock Second Derivatives and Electric Field Properties in a Solvent Reaction Field: Theory and Application. *J. Chem. Phys.* **1991**, *95*, 8991−8998.
(54) Wong, M. W.; Wiberg, K. B.; Frisch, M. J. Solvent Effects. 2. Medium Effect on the Structure, Energy, Charge Density, and Vibrational Frequencies of Sulfamic Acid. *J. Am. Chem. Soc.* **1992**, *114*, 523−529.
(55) Wong, M. W.; Wiberg, K. B.; Frisch, M. J. Solvent Effects. 3. Tautomeric Equilibria of Formamide and 2-Pyridone in the Gas Phase and Solution: An Ab Initio SCRF Study. *J. Am. Chem. Soc.* **1992**, *114*, 1645−1652.
(56) Guo, L.; Qi, C.; Zheng, X.; et al. Toward Understanding the Adsorption Mechanism of Large Size Organic Corrosion Inhibitors on an Fe(110) Surface Using the DFTB Method. *RSC Adv.* **2017**, *7*, 29042−29050.
(57) Oguike, R.; Kolo, A.; Shibdawa, A., et al. Density Functional Theory of Mild Steel Corrosion in Acidic Media Using Dyes as Inhibitor: Adsorption onto Fe(110) from Gas Phase. *ISRN Phys. Chem.* **2013**, *2013*, 1−19.
(58) Umar, B. A.; Uzairu, A. In-Silico Approach to Understand the Inhibition of Corrosion by Some Potent Triazole Derivatives of Pyrimidine for Steel. *SN Appl. Sci.* **2019**, *1*, No. 1413.
(59) Monkhorst, H. J.; Pack, J. D. Special Points for Brillouin-Zone Integrations. *Phys. Rev. B* **1976**, *13*, 5188−5192.
(60) Nosé, S. A Molecular Dynamics Method for Simulations in the Canonical Ensemble. *Mol. Phys.* **1984**, *52*, 255−268.
(61) Hoover, W. G. Canonical Dynamics: Equilibrium Phase-Space Distributions. *Phys. Rev. A* **1985**, *31*, 1695−1697.
(62) Hanwell, M. D.; Curtis, D. E.; Lonie, D. C.; et al. Avogadro: An Advanced Semantic Chemical Editor, Visualization, and Analysis Platform. *J. Cheminf.* **2012**, *4*, No. 17.
(63) Humphrey, W.; Dalke, A.; Schulten, K. VMD: Visual Molecular Dynamics. *J. Mol. Graphics* **1996**, *14*, 33−38.
(64) Momma, K.; Izumi, F. VESTA 3 for Three-Dimensional Visualization of Crystal, Volumetric and Morphology Data. *J. Appl. Crystallogr.* **2011**, *44*, 1272−1276.
(65) Huo, J.; Bradley, W.; Podolak, K.; et al. Triacetic Acid Lactone and 4-Hydroxycoumarin as Bioprivileged Molecules for the Development of Performance-Advantaged Organic Corrosion Inhibitors. *ACS Sustainable Chem. Eng.* **2022**, *10*, 11544−11554.
(66) Popova, A. Temperature Effect on Mild Steel Corrosion in Acid Media in Presence of Azoles. *Corros. Sci.* **2007**, *49*, 2144−2158.
(67) Naciri, M.; El Aoufir, Y.; Lgaz, H.; et al. Exploring the Potential of a New 1,2,4-Triazole Derivative for Corrosion Protection of Carbon Steel in HCl: A Computational and Experimental Evaluation. *Colloids Surf., A* **2020**, *597*, No. 124604.
(68) Li, X.; Deng, S.; Fu, H.; et al. Adsorption and Inhibition Effect of 6-Benzylaminopurine on Cold Rolled Steel in 1.0M HCl. *Electrochim. Acta* **2009**, *54*, 4089−4098.
(69) Loto, R. T. Corrosion Inhibition Effect of Non-Toxic A-Amino Acid Compound on High Carbon Steel in Low Molar Concentration of Hydrochloric Acid. *J. Mater. Res. Technol.* **2019**, *8*, 484−493.
(70) Venkatesan, P.; Anand, B.; Matheswaran, P. Influence of Formazan Derivatives on Corrosion Inhibition of Mild Steel in Hydrochloric Acid Medium. *J. Chem.* **2009**, *6*, No. 507383.
(71) Hegazy, M. A. A Novel Schiff Base-Based Cationic Gemini Surfactants: Synthesis and Effect on Corrosion Inhibition of Carbon Steel in Hydrochloric Acid Solution. *Corros. Sci.* **2009**, *51*, 2610−2618.
(72) Cheng, S.; Chen, S.; Liu, T.; et al. Carboxymenthylchitosan as an Ecofriendly Inhibitor for Mild Steel in 1 M HCl. *Mater. Lett.* **2007**, *61*, 3276−3280.
(73) Lebrini, M.; Lagrenée, M.; Traisnel, M.; et al. Enhanced Corrosion Resistance of Mild Steel in Normal Sulfuric Acid Medium by 2,5-Bis(N-Thienyl)-1,3,4-Thiadiazoles: Electrochemical, X-Ray Photoelectron Spectroscopy and Theoretical Studies. *Appl. Surf. Sci.* **2007**, *253*, 9267−9276.
(74) Okafor, P. C.; Zheng, Y. Synergistic Inhibition Behaviour of Methylbenzyl Quaternary Imidazoline Derivative and Iodide Ions on Mild Steel in H_2SO_4 Solutions. *Corros. Sci.* **2009**, *51*, 850−859.
(75) Khan, G.; Basirun, W. J.; Kazi, S. N.; et al. Electrochemical Investigation on the Corrosion Inhibition of Mild Steel by Quinazoline Schiff Base Compounds in Hydrochloric Acid Solution. *J. Colloid Interface Sci.* **2017**, *502*, 134−145.
(76) Singh, A. K.; Shukla, S. K.; Singh, M.; et al. Inhibitive Effect of Ceftazidime on Corrosion of Mild Steel in Hydrochloric Acid Solution. *Mater. Chem. Phys.* **2011**, *129*, 68−76.
(77) Shaban, S. M. N-(3-(Dimethyl Benzyl Ammonio)Propyl)-Alkanamide Chloride Derivatives as Corrosion Inhibitors for Mild Steel in 1 M Hcl Solution: Experimental and Theoretical Investigation. *RSC Adv.* **2016**, *6*, 39784−39800.
(78) Sukul, D.; Pal, A.; Saha, S. K.; et al. Newly Synthesized Quercetin Derivatives as Corrosion Inhibitors for Mild Steel in 1 M HCl: Combined Experimental and Theoretical Investigation. *Phys. Chem. Chem. Phys.* **2018**, *20*, 6562−6574.
(79) Zhang, Q. B.; Hua, Y. X. Corrosion Inhibition of Mild Steel by Alkylimidazolium Ionic Liquids in Hydrochloric Acid. *Electrochim. Acta* **2009**, *54*, 1881−1887.

(80) Robinson, V. Imaging with Backscattered Electrons in a Scanning Electron Microscope. *Scanning* **1980**, *3*, 15−26.
(81) Biesinger, M. C. Accessing the Robustness of Adventitious Carbon for Charge Referencing (Correction) Purposes in XPS Analysis: Insights from a Multi-User Facility Data Review. *Appl. Surf. Sci.* **2022**, *597*, No. 153681.
(82) Auciello, O.; Veyan, J.-F.; Arellano-Jimenez, M. J. Comparative X-Ray Photoelectron Spectroscopy Analysis of Nitrogen Atoms Implanted in Graphite and Diamond *Frontiers in Carbon* 2023; Vol. *2* DOI: 10.3389/frcrb.2023.1279356.
(83) Biesinger, M. C.; Payne, B. P.; Grosvenor, A. P.; et al. Resolving Surface Chemical States in XPS Analysis of First Row Transition Metals, Oxides and Hydroxides: Cr, Mn, Fe, Co and Ni. *Appl. Surf. Sci.* **2011**, *257*, 2717−2730.
(84) Beamson, G.; Briggs, D. R. *High Resolution XPS of Organic Polymers: The Scienta Esca300 Database*, 1992.
(85) Arellanes-Lozada, P.; Olivares-Xometl, O.; Likhanova, N. V.; et al. Adsorption and Performance of Ammonium-Based Ionic Liquids as Corrosion Inhibitors of Steel. *J. Mol. Liq.* **2018**, *265*, 151−163.
(86) El Faydy, M.; Benhiba, F.; About, H.; et al. Experimental and Computational Investigations on the Anti-Corrosive and Adsorption Behavior of 7-N,N′-Dialkyaminomethyl-8-Hydroxyquinolines on C40e Steel Surface in Acidic Medium. *J. Colloid Interface Sci.* **2020**, *576*, 330−344.
(87) Olasunkanmi, L. O.; Obot, I. B.; Kabanda, M. M.; et al. Some Quinoxalin-6-Yl Derivatives as Corrosion Inhibitors for Mild Steel in Hydrochloric Acid: Experimental and Theoretical Studies. *J. Phys. Chem. C* **2015**, *119*, 16004−16019.
(88) Goulart, C. M.; Esteves-Souza, A.; Martinez-Huitle, C. A.; et al. Experimental and Theoretical Evaluation of Semicarbazones and Thiosemicarbazones as Organic Corrosion Inhibitors. *Corros. Sci.* **2013**, *67*, 281−291.
(89) Yan, Y.; Li, W.; Cai, L.; et al. Electrochemical and Quantum Chemical Study of Purines as Corrosion Inhibitors for Mild Steel in 1M HCl Solution. *Electrochim. Acta* **2008**, *53*, 5953−5960.
(90) Raviprabha, K.; Bhat, R. S. Corrosion Inhibition of Mild Steel in 0.5 M HCl by Substituted 1,3,4-Oxadiazole. *Egypt. J. Pet.* **2023**, *32*, 1−10.
(91) Boughoues, Y.; Benamira, M.; Messaadia, L.; et al. Experimental and Theoretical Investigations of Four Amine Derivatives as Effective Corrosion Inhibitors for Mild Steel in HCl Medium. *RSC Adv.* **2020**, *10*, 24145−24158.
(92) Cao, Z.; Tang, Y.; Cang, H.; et al. Novel Benzimidazole Derivatives as Corrosion Inhibitors of Mild Steel in the Acidic Media. Part II: Theoretical Studies. *Corros. Sci.* **2014**, *83*, 292−298.
(93) Lukovits, I.; Kálmán, E.; Zucchi, F. Corrosion Inhibitors—Correlation between Electronic Structure and Efficiency. *Corrosion* **2001**, *57*, 3−8.
(94) Shaw, P.; Obot, I. B.; Yadav, M. Functionalized 2-Hydrazinobenzothiazole with Carbohydrates as a Corrosion Inhibitor: Electrochemical, XPS, DFT and Monte Carlo Simulation Studies. *Mater. Chem. Front.* **2019**, *3*, 931−940.
(95) Obot, I. B.; Gasem, Z. M. Theoretical Evaluation of Corrosion Inhibition Performance of Some Pyrazine Derivatives. *Corros. Sci.* **2014**, *83*, 359−366.
(96) Kabanda, M. M.; Obot, I. B.; Ebenso, E. E. Computational Study of Some Amino Acid Derivatives as Potential Corrosion Inhibitors for Different Metal Surfaces and in Different Media. *Int. J. Electrochem. Sci.* **2013**, *8*, 10839−10850.

https://doi.org/10.1021/acs.langmuir.5c00183
Langmuir 2025, 41, 8407−8423